PCCP

ROYAL SOCIETY OF CHEMISTRY

PERSPECTIVE

View Article Online
View Journal | View Issue

Cite this: *Phys. Chem. Chem. Phys.*, 2022, **24**, 8553

Neutron reflection and the thermodynamics of the air–water interface

Jeffrey Penfold*[ab] and Robert K. Thomas[b]

By means of isotopic substitution, measurements of the neutron reflectivity (NR) from a flat water surface generally give model independent measurements of the amount of a chosen solute at the surface irrespective of whether the layer is a mixture or whether there is any aggregation in the bulk solution. Previously, adsorption at air–water interfaces has been determined by applying the Gibbs equation to surface tension (ST) measurements, which requires assumptions about the composition of the surface and about the activity of the solute in the bulk, which, in turn, means that in practice the surface is assumed to consist of the pure solute or of a mixture of pure solutes, and that the activity of the solute in the bulk solution is known. The use of NR in combination with ST-Gibbs measurements makes it possible to (i) avoid these assumptions and hence understand several patterns of ST behaviour previously considered to be anomalous and (ii) to start to analyse quantitatively the behaviour of mixed surfactants both below and above the critical micelle concentration. These two developments in our understanding of the thermodynamics of the air–water interface are described with recent examples.

Received 5th January 2022,
Accepted 14th March 2022

DOI: 10.1039/d2cp00053a

rsc.li/pccp

1 Introduction

A surface consists of a thin layer of matter, often an atomic or molecular monolayer, and it would be expected that such a layer would most effectively be probed by whatever particle or electromagnetic radiation is most sensitive to short range structure. Of the three main structural probes for exploring condensed matter at the molecular level, *i.e.* electrons, X-rays and neutrons, neutrons interact by far the most weakly, as is illustrated by the comparison of diffraction from a surface. Low energy electron diffraction can determine the structure of the surface of a single crystal with high accuracy whereas neutron diffraction requires a very high surface area of material, *i.e.* a powdered and therefore more disordered sample, to detect any diffraction from adsorbed material, and can therefore only be applied in a relatively approximate way to a small number of systems. However, the compensating advantage of the weak

[a] *ISIS Facility, Rutherford Appleton Laboratory, Harwell Campus, Didcot, Oxon, UK. E-mail: jeffrey.penfold@stfc.ac.uk*
[b] *Physical and Theoretical Chemistry Laboratory, University of Oxford, South Parks Road, Oxford, UK*

Jeffrey Penfold

Jeff Penfold is an Emeritus Fellow (formerly Senior Fellow) at STFC's Rutherford Appleton Laboratory, and a Visiting Professor at the Physical and Theoretical Chemistry Laboratory, Oxford. His joint research with Bob Thomas in Oxford has a wide programme in colloid and interface science. His research, exploiting neutron scattering techniques to study surfactant and mixed surfactant adsorption and self-assembly, biosurfactants, polymer-surfactant mixtures, functionalised surfaces, and processing, has produced > 400 publications.

Robert K. Thomas

Bob Thomas is Emeritus at the Chemistry Department at Oxford, where he has spent his research career since 1966 and where he started in the field of neutron scattering 47 years ago. He continues a joint programme of research with Jeff Penfold, which is presently focussed on using neutron scattering techniques to explore the surface behaviour of surfactants, polymer/surfactant systems, surfactant mixtures and biosurfactants. He is a Fellow of the Royal Society.

interaction of neutrons with matter is that neutron beams can access buried surfaces because they pass easily through a vapour phase (the air–water (A–W) interface is a buried interface for electrons) and reasonably easily through many solids and liquids. A feature of X-rays and neutrons that can be used to enhance the signal from such a buried interface is their strong and sometimes total reflection from a flat surface when close to grazing incidence. In the vicinity of total reflection the reflectivity is sensitive to the variation of composition along the direction normal to the surface. The reflection of light is also sensitive to refractive index but the relationship between refractive index and molecular structure is complicated. This can only be overcome partially by the use of ellipsometry, which exploits the difference in refractive index for two states of polarization. For neutrons and X-rays, the respective refractive indices depend only on the atomic composition, which is simple. X-ray beams are much more intense than neutron beams and this might suggest that low angle X-ray reflection would be more sensitive than low angle neutron reflection. However, nature has been extraordinarily kind to neutron scatterers in that the scattering of neutrons by H and D nuclei is opposite in phase and sufficiently strong that the contribution of O to the scattering from water is dominated by H or D so that total *external* reflection occurs at the air–D_2O interface whereas total *internal* reflection occurs at the H_2O–air interface. At a composition of about 8 mol% of D_2O (null reflecting water or NRW) this phase difference cancels so that there is no reflection at all from an air–NRW interface. There is just a low level background from a mix of incoherent scattering (spin fllipped neutrons) and multiple scattering from the short range liquid structure. This background is 1–5 $\times$ 10^{-6} times total reflection whereas the signal from a typical perdeuterated surfactant layer in NRW would range up to 10^{-3} or higher depending on the composition and/or how low an angle the reflectivity measurement can reach.

Neutron reflection (NR) has the complication that it requires a neutron beam from either a reactor or a spallation source, but at the level of the user both the experiment and the analysis of the data are relatively simple. For a horizontal liquid–air interface the solution is typically contained in a Teflon trough in a sealed and thermostatted container with quartz windows. The illuminated area of the surface of the liquid is typically about 10 $\times$ 5 cm^2 and its volume 25–35 cm^3. The beam is usually polychromatic, in which case the sample is stationary, and sometimes monochromatic, in which case the sample moves up and down and the beam is controlled by neutron mirrors. Following subtraction of the low level of background incoherent scattering mentioned above, the reflectivity is obtained as a function of the momentum transfer, κ, defined by

$$\kappa = \frac{4\pi \sin\theta}{\lambda} \tag{1}$$

where θ is the angle of incidence and λ is the wavelength. The data is usually calibrated with respect to pure D_2O. The measurement time for a complete reflectivity profile depends on the strength of the neutron source, the configuration of the reflectometer and the level of deuteration of the surfactant or polymer but typically varies from a few minutes to about an hour.

Before considering how NR data is analysed we examine some features of the surface of surfactant solutions that are relevant to the determination of the surface excess, which is our primary concern in this review. An adsorbed layer at the A–W interface may or may not be laterally uniform. If island formation occurs it will only affect the NR directly if the lateral dimension of the islands is larger than the in-plane coherence length of the neutrons, which in turn depends on the optics of the experimental set up, but is of the order of 10^4 Å. The layer would therefore have to be close to phase separation for anything other than an average lateral structure to be observed. If there is surface phase separation for a single amphiphile the reflectivity of an air–NRW surface half covered by a monolayer of deuterated surfactant would be approximately double that of the same amount of uniformly spread surfactant. Parallel considerations apply to mixtures of protonated and deuterated surfactants. The average thickness of an adsorbed layer depends on the length and orientation of the molecules and their thermal motion (capillary waves). A reasonable assumption is that the profile of the deuterium labelled part of the surfactant along the surface normal direction, which is what is essentially ''seen'' by NR, is Gaussian, *i.e.*

$$\rho = \rho_0 \exp\left(-\frac{4z^2}{\sigma^2}\right) \tag{2}$$

where z is the distance along the surface normal, σ is the full width at $1/e$ of the maximum, and ρ, the scattering length density, is

$$\rho = \sum_i n_i b_i \tag{3}$$

where b_i and n_i are are the scattering lengths and number densities of the constituent nuclei (values of b are accurately known for most isotopes.) The negative value of b for hydrogen, and the positive values for deuterium and carbon are such that saturated hydrocarbon chains adsorbed at the air–NRW interface are close to invisible while the equivalent deuterocarbon chains give a very strong signal, and this is the basis for measurements of the surface composition of surfactant mixtures. Most small counterions are also close to invisible when compared with a deuterocarbon fragment. Hence NR generally only observes the surfactant ion.

It is instructive to illustrate the quantitative analysis of the NR data by using an approximate model to analyse the reflectivity from a solution of perdeuterated surfactant in NRW. The kinematic approximation gives the reflectivity in terms of the Fourier transform of eqn (2) and leads to the following equation relating the surface excess and the reflectivity:[2–4]

$$\ln\left(\frac{\kappa^2 R}{16\pi^2}\right) \simeq \Gamma_m - \kappa^2\sigma^2 \tag{4}$$

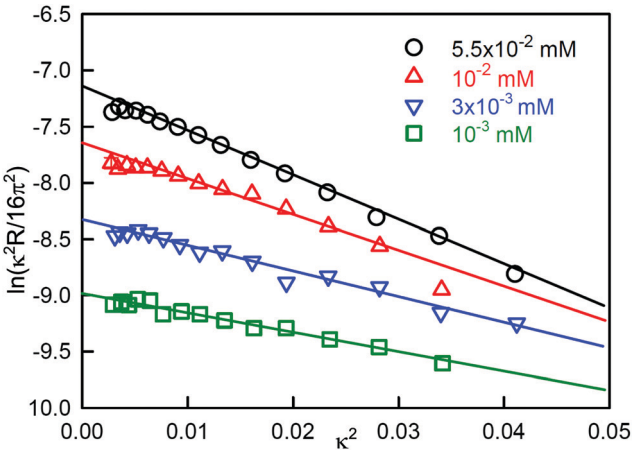

Fig. 1 Linear extrapolation of reflectivity data for $C_{12}E_3$ solutions to obtain the surface excess at various concentrations using eqn (4). Data redrawn from Lu *et al.*[1]

where the molar surface excess, Γ_m, is

$$\Gamma_m = \frac{\sigma\rho_0\pi^{1/2}}{2N_A} \quad (5)$$

The approximate eqn (4) can be used to analyse the reflectivity data for a typical deuterated surfactant to a good level of accuracy, as demonstrated in Fig. 1 for $C_{12}D_{25}$ $(O\text{-}C_2H_4)_3OH$ ($dC_{12}E_3$) in NRW. Although this is only an approximate calculation, it demonstrates clearly that in the case of a simple surfactant layer the values of Γ_m and σ for the layer are decoupled into intercept and gradient respectively. In addition, at the concentrations typical of such studies, Γ_m can be identified with the surface excess determined from ST-Gibbs equation measurements, because the position of the dividing surface used to define Γ_{ST} will be on the dilute solution side of the monolayer. This was confirmed for $C_{12}E_3$ by the close agreement of the intercepts in Fig. 1 with the independent ST results.[3] This close agreement and those for related nonionic systems also indicates that isotope effects are relatively insignificant in these systems.[5] In particular cases this can be further confirmed by comparing either ST or NR measurements on the pure deuterated surfactant and a 50 : 50 molar mixture of perdeuterated and hydrogenated surfactant.

Fig. 1 and eqn (4) show that the surface excess of a perdeuterated surfactant at the A–NRW interface can be determined relatively directly using NR. Since most surfactants with a hydrocarbon tail give rise to only a small signal when adsorbed at the surface of NRW the same principle can be used to measure the surface excess of a deuterated surfactant in a mixture with one or more hydrogenated surfactants. Most commercial surfactant formulations rely on cooperative interactions of the surfactants in the mixture. Such cooperative (or anti-cooperative) effects are expected to lead to deviations of the composition from their ideal values but, until the advent of NR, they have been difficult to measure below the critical micelle concentration (CMC) and more or less impossible to measure above the CMC, which is the concentration at which they are often used. Provided that there is no sublayer structure, which is relatively easily identified by NR itself, measurement of the surface excess of a single deuterated surfactant in the presence of others is feasible down to an adsorbed fraction of about 5% of a monolayer. The signal can be improved and isotope effects can be assessed by using different combinations of hydrogenated and deuterated samples, *e.g.* single deuterated or pairs of deuterated surfactants can be used to study a ternary mixture and the final compositions determined by solving the resulting set of simultaneous equations to obtain the individual excesses.

The separation of the roughness from the surface excess and the definition of NR and ST surface excesses become more difficult for more soluble surface active species such as short chain alkanols and phenols. This results from a combination of the lower scattering length density of the adsorbed species and the non-zero scattering length density of the underlying solution. For example, there has recently been some discussion by Nguyen *et al.* on the significance of sublayer adsorption for the measured adsorption isotherm of hexanol in water.[6–8] The authors attributed a low value of the measured surface excess for hexanol to their sum frequency generation (SFG) measurements not probing the inner part of the surface. A direct comparison can be made between NR and SFG for this case. Thus, Li *et al.*[9] found excellent consistency between the NR excess and that determined from ST using the Gibbs equation up to the hexanol saturation limit of 60 mM. The SFG measurements gave a value of 6.5 μmol m^{-2} at a bulk concentration of 35 mM, where the interpolated value from NR (and ST) was only 5.5 ± 0.2 μmol m^{-2}. In addition, Li *et al.* found a thickness of the hexanol layer of 18 ± 2 Å at maximum coverage, treated as a uniform slab. Although this is larger than the length of a hexanol molecule, it does not indicate the presence of a significant sublayer because the measured NR value necessarily includes all the thermal roughness. The SFG measurement in this case overestimates the coverage and there is no anomalous sublayer. However, for the shorter phenol molecule, Li *et al.*[10] did find an unexpectedly large layer thickness of 19 ± 2 Å close to the solubility limit, a feature which has not yet been explained but which may indicate some deeper structure to the layer as a whole. In general, the depth of penetration of NR is such that in normal experimental conditions NR can respond to excess surfactant in the sublayer region, *e.g.* in the form of multilayers. The comparisons above have been made for nonionic species. There are two complications in making such comparisons for ionic species. First NR is not directly sensitive to small counterions, although it does respond to counterions with sufficiently high scattering lengths, *e.g.* tetramethyl ammonium[11] or tosylate.[12] and, secondly ST is sensitive to both any enhanced adsorption of a counterion and to the extra change in entropy from its adsorption. This is an area where the combination of the two techniques is effective and is therefore part of the following discussion.

There are three main contributions of NR to the understanding of the thermodynamics of adsorption at the A–W interface, (i) the broadening of the range of application of the

Gibbs equation, (ii) the interpretation of the interfacial properties of multi-component mixtures, and (iii) the provision of structural information for statistical thermodynamic models of the interface. Although NR has also contributed to the general understanding of the structure of other types of interface involving liquids, *i.e.* solid–liquid and liquid–liquid, this has mostly been less specifically concerned with thermodynamic issues. This review concerns just the first two topics, *i.e.* the coupling of NR to the interpretation of the Gibbs equation at the A–W interface and the understanding of the mixing of surfactants at the same interface.

2 Neutron reflection and the Gibbs equation

For many years the two main applications of the Gibbs equation have been (i) that it has been more or less the only means of determining adsorption isotherms of solutes at the A–W interface, and (ii) that it converts models of adsorption into the surface tension (ST) behaviour of A–W and oil–water (O–W) interfaces, the second of which is obviously important for many practical applications, *e.g.* cleaning and coating surfaces. In the first of these applications, the equation is a typical thermodynamic equation in that it creates an opportunity for measurements of one easily accessed physical quantity (here the ST) to be used to derive the value of a different physical quantity that is hard to access (here the surface excess, Γ). Its simplest form is that for a nonionic solute at an A–W interface,

$$-\mathrm{d}\sigma = RT\Gamma d\ln a \qquad (6)$$

where σ is the ST and a is the activity of the solute in the bulk solution. Just as in any other thermodynamic measurement, the value of Γ determined from the variation of σ with ln a is correct only if the composition of the surface excess is known, *i.e.* if the surface layer is composed only of the supposed solute, solvent (and air). However, the Gibbs equation offers no means of verifying the composition of the surface layer. There have been many important discussions about how to subdivide solute, solvent and air (or other solvent) at A–W or O–W interfaces (see, for example, Radke[13] and Ikeda[14]) but only relatively recently has it become possible to make independent measurements of the composition of a liquid interface. Of the methods that have so far been used for this purpose NR is particularly direct, and this has led to the identification and elucidation of a number of problems concerning the composition of layers at the A–W interface, and hence to the explanation of several *apparent*[6,15] anomalies in the application of the Gibbs equation.[16–18]

A further valuable feature of the NR measurement is that it is normally independent of the state of the underlying bulk solution and adsorption can therefore be studied in concentration ranges where the activities of the components of the solution are incompletely known and where there is then insufficient information for the Gibbs equation to be correctly applied. Examples are measurements above the CMC, measurements at low concentrations where depletion may occur, measurements on systems where there is unexpected association or ionization of the solute, or where there is polydispersity. Situations often arise in these systems where the independent determination of surface excess leads to a way of applying the Gibbs equation more correctly. The first part of this review examines situations where such a combination leads to a better understanding of the particular system and the second part examines adsorbed mixtures.

2.1 Ionic surfactants and nonionic impurities

Impurities are common in surfactant solutions. The most troublesome ones tend to be nonionic low solubility species that are very surface active. Apart from the need to eliminate them for a better understanding of the surfactant being studied, such species are also commonly used in surfactant formulations as, for example, perfumes, coatings, or disinfectants. This involves their solubilization into an aqueous formulation from which they end up being deposited as a coating on the target material after the detergent has been rinsed off. An understanding of the nature of the various processes involved would obviously be valuable. Part of this is understanding surface mixtures but another part is that the additive (or impurity) usually has an adsorption and micellization behaviour quite different from that of the surfactant itself. The presence of such a species requires a second term to be added to eqn (6) to give

$$-\mathrm{d}\sigma = RT\Gamma_s d\ln a_s + RT\Gamma_i d\ln a_i \qquad (7)$$

where the subscripts s and i refer to the surfactant and impurity (or additive) respectively and a_i may or may not be proportional to a_s. By measuring the ST as a function of varying a_s at constant, and *vice versa* it is possible to determine the surface excesses of the separate components,[19] which is now routinely done by NR on surfactant mixtures[20] as discussed in a later section. However, this is not always possible when species i is an impurity. The effect of the impurity is therefore to make it difficult or impossible to use ST and the Gibbs equation to determine the surface excess.

The most widely studied example is the system sodium dodecylsulfate (SDS)-dodecanol where dodecanol is often formed by hydrolysis of the SDS. The effect of traces of dodecanol is qualitatively well understood.[21] The ST of pure dodecanol in water falls to a constant and low value at its low solubility limit. Dodecanol is also solubilized into SDS micelles and, at concentrations well above the CMC of SDS, the solubilization lowers the dodecanol monomer concentration so that its effect on the ST becomes negligible. The intermediate behaviour depends on the pattern of co-micellization of dodecanol and SDS, which in turn depends on the specific details of the interaction of dodecanol and SDS, which are not known. NR has been used to measure the surface excesses of each component as a function of composition and concentration[22] and Li *et al.*[18] later used these and the integrated version of eqn (7) to make an approximate quantitative interpretation of the resulting ST. As expected from the discussion above the directly measured surface excess of dodecanol passes through a

maximum just below the CMC of SDS and the amount of dodecanol slowly declines to a low value as it is incorporated into the SDS micelles. Corresponding to the strong maximum in the adsorption of dodecanol there is a sharp minimum in the ST, somewhat below the normal CMC.

A better defined example occurs for the surfactant dodecanoyl L-carnitine ($C_{12}CO_2$-LC), which behaves similarly to SDS/dodecanol in that the impurity is formed by hydrolysis. However, from the point of view of understanding the phenomenon, it has the advantage that the solubility of the impurity can be varied by changing the pH, which gives greater clarity to the processes described above for SDS-dodecanol. C-LC is a zwitterionic surfactant that hydrolyses to give dodecanoic acid and the amino-acid L-carnitine.[23] Dodecanoic acid has a low solubility that is strongly affected by pH, as shown in Fig. 2(c). Its effect on the ST is largest at low pH, where its solubility is well below the CMC of $C_{12}CO_2$-LC, but negligible at pH 7 where its solubility limit is much higher. It therefore causes a sharp minimum in the ST at pH = 2 but the minimum more or less disappears at pH = 7 (Fig. 2(a)). The total surface excess of acid + $C_{12}CO_2$LC, as measured by NR, passes through a sharp maximum at pH = 2 before reaching a plateau, but proceeds directly to a plateau at pH = 7 (Fig. 2(b)). The level of the adsorption on the two plateaus in Fig. 2(b) is, however, quite different, being about 10% higher at pH = 2. At pH 2 the $C_{12}CO_2$LC is a cationic surfactant because the carboxylic group

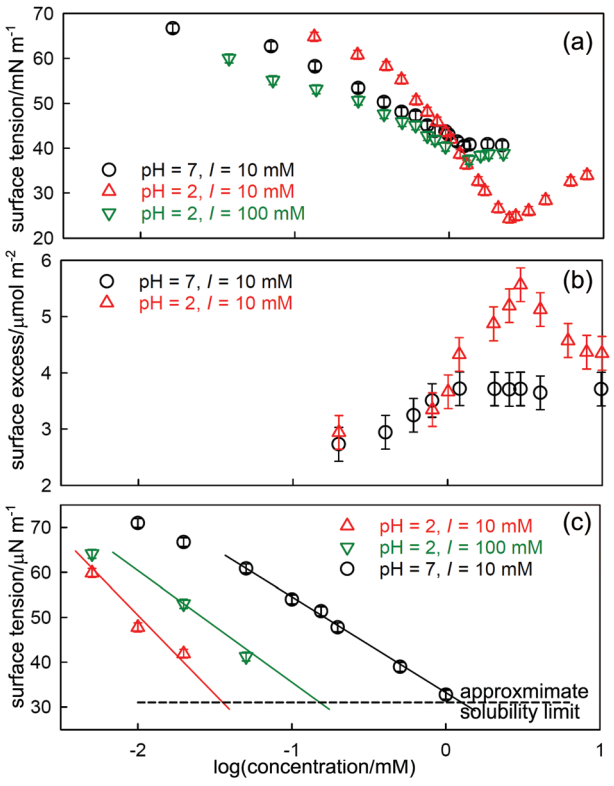

Fig. 2 Effects of hydrolysis of dodecanoyl-L-carnitine on its ST behaviour, (a) ST at pH of 2 and 7 and different ionic strengths (I), (b) the total surface excess (dodecanoic acid and $C_{12}CO_2$LC), and (c) the ST of dodecanoic acid at different pH. Data redrawn from Liu *et al.*[23]

is a weak acid, but at pH 7 it is zwitterionic, *i.e.* overall neutral. The adsorbed layer would therefore be expected to be more closely packed at pH 7 than at pH 2, but this is the opposite of what is observed. This indicates that the higher adsorption observed at pH 2 must result from co-adsorption of the neutral acid with the $C_{12}CO_2$LC. The difference in the state of ionization of the $C_{12}CO_2$LC was further confirmed by neutron small angle scattering (SANS) from the micelles, which exhibits a charge interaction peak at pH 2 but not at pH 7. A large increase in ionic strength also raises the solubility of dodecanoic acid and hence the concentration at which it reaches a low ST. This also removes the minimum in the ST at pH 2, which illustrates why adding electrolyte is a useful means of reducing the effects of nonionic impurities in such measurements.[24]

2.2 Counterion impurities in ionic surfactants

Any ionic material adsorbed at the A–W interface must form a neutral layer. For a surfactant MX_z eqn (7) therefore becomes

$$-d\sigma = RT\Gamma_M d\ln a_{M^{z+}} + zRT\Gamma_X d\ln a_{X^-} = -PRT\Gamma_{MX_z} d\ln a_{\pm} \quad (8)$$

where $a_{\pm}$ is the mean activity of MX_z. The prefactor, P, equals $(z + 1)$, and is 2 for a 1:1 electrolyte and 3 for a divalent counterion, which substantially changes the gradient of a Gibbs plot (σ against $\ln c$). However, the main difference is usually that ions of higher charge decrease the CMC so that the Gibbs plot is displaced to lower concentrations. This change is large when a monovalent counterion is replaced by one of higher charge as in the adsorption of the ethylhexylsulfosuccinates of sodium and calcium (NaAOT and $Ca(AOT)_2$).[25,26] The surface activity of $Ca(AOT)_2$ is much higher than NaOT, which means that low levels of contamination by Ca^{2+} significantly influence the behaviour of the ST at such low concentrations that it is extremely difficult to eliminate the effect of the ionic impurity. The effect can be identified by following the changes of ST with concentration of surfactant at constant electrolyte and of electrolyte at constant surfactant, as can be seen from eqn (8). Thus, for perfluorooctanoates, Shinoda and Nakayama[27] examined the surface behaviour at constant surfactant and varying electrolyte concentration with various cations, H^+, $K^+$and Ba^{2+}, and found that in all three cases the adsorption of the counterion was only about half that of the surfactant ion. Hall *et al.*[28] later gave a more complete analysis of the theory of such a measurement, which included the calculated activity coefficients and a contribution from the co-ion, and also concluded that there was an apparent shortfall in the coverage of counterion. Fluorine atoms scatter neutrons strongly and it is relatively easy to determine the surface excess of the fluorooctanoate ion directly by NR. An *et al.*[29] used NR to measure the surface excesses of the Na^+, $Cs^+$and H^+forms of the perfluorooctanoate, without the complicating effect of added electrolyte, and showed that the ST + Gibbs determination underestimated the directly measured surface excess of surfactant by about 30%. This can only be explained as contamination with more strongly binding ions, *i.e.* ions of higher valence. That Ca^{2+} is

the likely contaminant was shown by using EDTA to sequester any Ca^{2+} ions present, which removed the anomaly. More recently, Lunkenheimer *et al.* have refined the purification of the fluorooctanoates to a level where divalent ion impurities can be removed from this system.[30]

2.3 Depletion in dilute solution

While depletion is not really the concern of thermodynamics, it sometimes leads to an apparent break in a Gibbs plot and there are several examples where a depletion break has been interpreted as micellization. Since the conditions of NR and ST measurements are different, the onset of depletion will also tend to occur at different concentrations. The incorporation of NR data into the integrated Gibbs equation and its comparison with the measured ST can be used to distinguish such breaks. Depletion can also affect the ST behaviour of polymers, but in a more complicated way. Since they are polydisperse, their STs are generally time dependent, *e.g.*,[31] and measurements are often made at low *molar* concentrations where depletion is probable.

A simple estimate of how much surfactant is required to cover the A–W surface of a container used for ST measurements suggests that it is typically equivalent to less than about 10^{-7} M in the bulk solution and such low concentrations are generally avoided. However, the direct comparison of NR and ST measurements shows that in many cases depletion of the solute occurs at significantly higher concentrations than 10^{-7} M. If depletion is only to the A–W interface NR can give the required correction to the bulk concentration directly using the measured excess and the geometry of the containment vessel. NR measurements generally use Teflon troughs and, since hydrocarbon surfactants do not normally adsorb on Teflon and the technique of NR requires no physical interaction with the surface other than the reflection of neutrons, a correction for depletion is relatively easy to make. On the other hand, many ST measurements use glass containers and often also a metal ring or metal plate to interact with the surface, on all of which adsorption of surfactants is expected to be strong so that the depletion is larger than just the loss to the A–W interface. This loss is therefore expected to be greater than in NR and can cause the ST-concentration relation to become uncertain at concentrations of 10^{-6} M or even higher, depending on the exact methodology of the measurement. The effect on the Gibbs plot will then be that it becomes concave up in the region where depletion starts, *i.e.* there is an apparent *increase* in coverage as the concentration is lowered. Such a change is not allowed thermodynamically unless bulk aggregation occurs in the higher concentration range.

Since depletion is unlikely to be the same in ST and NR experiments, the two techniques should give different results in any region of depletion. The effect is clear in NR and ST data for several different systems, of which two are shown in Fig. 3. In (a) and (c) the line represents the ST calculated from NR, with (a) being the results for a laboratory synthesized poloxamer ("Pluronic"), $E_{23}P_{52}E_{23}$, and (c) the results for a monodisperse poly(vinylmethylether) (PVME) with a MW of 4k. In both cases,

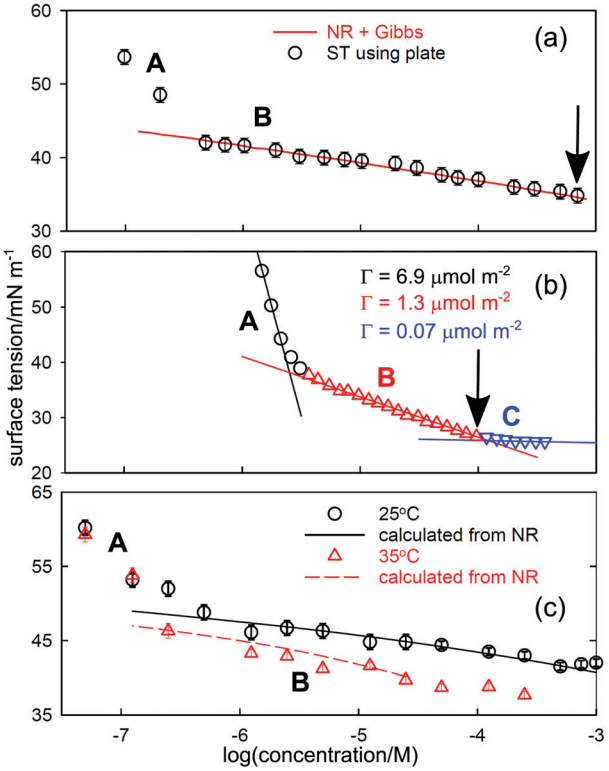

Fig. 3 Surface tension behaviour of aqueous solutions of (a) the poloxamer $E_{23}P_{52}E_{23}$, (b) the cationic double chained surfactant $C_{16}C_{12}$DAB, and (c) poly(vinylmethylether) of MW 4k. Region A is where surfactant is lost from the bulk solution by depletion to the various surfaces. In region B the calculated line uses NR and the integrated Gibbs equation in (a) and (c) but is the usual Gibbs plot in (b). The correct CMC in each case is marked by an arrow. The data are replotted from (a) Vieira *et al.*,[32] (b) Phan *et al.*,[33] and (c) An *et al.*[34]

the ST calculated for region B uses the NR measurements and the appropriate prefactor of one in the Gibbs equation. The measured excesses from NR extend to concentrations below the low concentration break point, as shown by the calculated lines in the two figures and they do not agree with the ST measurements. Since there is also little indication of depletion in the NR results below the break point the problem must lie in the ST and only depletion can explain the shape of the ST curve. It is not essential to have parallel NR measurements to establish that a given ST curve is affected by depletion. Thus, the low concentration break in the ST behaviour of for hexadecyl–dodecyl–dimethyl bromide ($C_{16}C_{12}$DAB) in Fig. 3(b) has been attributed to a second CMC at 0.003 mM by Phan *et al.*[33] and, assuming that the surfactant is fully dissociated in the most dilute region A, the surface excess in region A is 6.9 μmol m^{-2}, which is anomalously high. The value of the CMC is much lower than the CMC of 0.04 ± 0.02mM determined by Tucker *et al.*[35] for the related, but more hydrophobic compound diC_{16}DAB using both ST and NR. Tucker *et al.* also used NR to determine a surface excess of 2.6 ± 0.1 μmol m^{-2} at the CMC of 0.04 mM. In addition they measured a surface excess of 1.3 μmol m^{-2} directly with NR at a concentration of 0.003 mM. This agrees exactly with that from Phan *et al.*'s slope in region B

just below the A–B break in Fig. 3(b). Thus, the ST behaviour is only consistent with the intersection of regions A and B being the onset of depletion. The anomalous "CMC" for $C_{16}C_{12}$DAB in Fig. 3(b) is also at a substantially higher concentration than in (a) and (c). This difference may result from the number of moles removed by depletion being significantly larger for the smaller surfactant than for the two polymers. A comparable concentration depletion occurs in the surfactant Tween 60, for which the CMC was found to be 0.05 mM.[36]

Depletion is presented above as a type of false equilibrium, *i.e.* at long measurement times all the surfaces have equilibrium adsorbed amounts even if they are depleted, although there would necessarily be some variation from system to system. However, for polymer adsorption, since diffusion of polymers to the surface can be relatively slow, the equilibration times of the different MW species with the surface may also be "polydisperse". This is potentially particularly troublesome in that short and long measurement times may be dominated by different MW fractions. The time dependence of polymer ST is well known and attempts have been made to demonstrate by direct measurement of the surface excess that polymer adsorption obeys the Gibbs equation. Thus, deFeijter and Benjamins[37] found that the surface excesses from ST of a series of PVA (copolymers of vinyl alcohol and vinyl acetate), with MWs from 40k to 200k, were about 6× the value from ellipsometry, which they attributed to polydispersity. Comparison of NR and ST results from different MWs of PEO showed that the onset of depletion was at a concentration of about 3× lower for 20k than for 87k.[16] This is a second example that suggests that the molar depletion can be reduced for species with a larger adsorbed area.

2.4 Adsorption above the critical Micelle concentration

The application of the Gibbs equation to the ST of surfactant solutions at concentrations above the CMC requires values of the activity, which is substantially different from the concentration and not easy to determine experimentally, although the abrupt onset of the change is an excellent method for determining the CMC. The most completely studied surfactant above its CMC is SDS, for which the ST, the surface excess and the mean activity have all been independently measured and the combined results analysed by Xu *et al.*[17] Over a range of concentration from the CMC at about 8 mM up to about 6 × CMC (50 mM) the ST drops by about 3 mN m^{-1}, or 7.5%[38] and the surface excess correspondingly increases from a mean value of 3.9 to 4.6 μmol m^{-2} or 18%.[17] Combination of these results in the Gibbs equation gives a change of about 17% in the mean activity of SDS over this concentration range. Two sets of direct measurements of the mean activity by Sasaki *et al.*[39] and Cutler *et al.*[40] give corresponding changes of 15% and 10% respectively. The agreement is sufficient to demonstrate that for SDS the Gibbs equation is obeyed above the CMC and that the gradient of a Gibbs plot above the CMC is not zero, as it would be above a true phase change, but it is much lower than below the CMC.

An advantage of NR as a probe of the A–W interface is that it gives some structural information in addition to the surface excess, although at a lower level of accuracy. The resolution is sufficient to show that for SDS the increase in coverage measured by NR is all in the monolayer. However, for C_{14}TAB NR measurements of the layer structure above the CMC indicate that extra adsorption above the CMC is in the form of a micellar or fragmented lamellar type of layer with an intervening layer of water separating it from the monolayer.[41] The extra surface excess is about 10% at about 50 × CMC, similar to that for SDS, and there is a correspondingly similar drop of about 4 mN m^{-1} in the ST. However, the nature of the underlying adsorption must change from the mechanism below the CMC in that it must be driven by micelle-monolayer interaction rather than by simple amphiphilicity. Nevertheless, the underlying unit in the extra adsorbed sublayer must still have a stoichiometry that preserves surface neutrality. Unfortunately, there are no activity data to demonstrate the validity of the Gibbs equation for this case. The use of NR to examine surfaces above the CMC opens up an important area of research on mixtures of surfactants which is discussed further below.

2.5 Adsorption of multivalent ions and surfactants

We have already shown how trace quantities of ionic impurities seriously interfere with the application of the Gibbs equation to surfactants. More recently, the controlled addition of higher concentrations of multivalent ions to oppositely charged surfactant ions has identified several new patterns of A–W interfacial behaviour. The multivalency can be on a single atom, *i.e.* a metal ion, or distributed over a more extended structure, from an anion such as a sulphate ion through oligoions to a polyelectrolyte. The precipitating effect of ions such as Ca^{2+} and Mg^{2+} on anionic surfactant species is well known in connection with hard water. However, recent experiments with a wider range of cations, especially Al^{3+}, have shown that such ions can induce an intermediate range of behaviour in many anionic surfactants, in which the surface behaviour is enhanced[42] and layered structures form immediately below the surface,[43–46] even in common surfactants such as AOT[47] and SDS.[48] Most of these involve Al^{3+} as the multivalent ion, but the effect can also be observed with Ca^{2+} [49,50] and trivalent ions other than Al^{3+}.[51] The effect is unexpected in that the multilayered surface structures often occur in concentration ranges where there seems to be no parallel aggregation in the bulk solution. An example is the surfactant sodium decyl diethylene glycol sulfate (SCSS).

Fig. 4(a) shows the NR profiles from the A–W surface of mixtures of $SC_{10}E_2S$ at a constant concentration of 5 mM $SC_{10}E_2S$ (about CMC/2) following the addition of small amounts of $AlCl_3$, which is completely hydrolysed to Al^{3+} ions at these low concentrations. At zero $AlCl_3$ the $SC_{10}E_2S$ shows a reflectivity typical of a monolayer and this is enhanced by the addition of about 1 mol% of $AlCl_3$ (0.05 mM). The featureless decay of the reflectivity of these two profiles is typical of the usual monolayer of surfactant, which we designate as S_0. However, at slightly higher concentrations of $AlCl_3$ the reflectivity shows a distinct single fringe, which becomes a double fringe at about 3 mol% $AlCl_3$. The fringe is characteristic of a

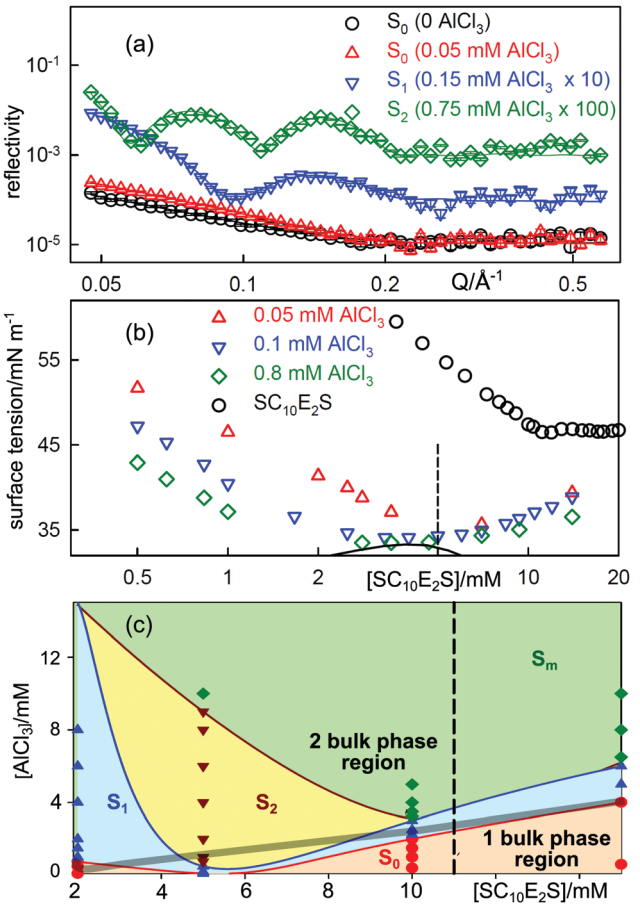

Fig. 4 Stratification of solutions of the surfactant $SC_{10}E_2S$ by $AlCl_3$ at the A–W interface. (a) Evolution of fringes in the neutron reflectivity of a 5 mM solution of $SC_{10}E_2S$ as $AlCl_3$is added. (b) ST behaviour of $SC_{10}E_2S/AlCl_3$ mixtures. The dashed line corresponds to the surfactant concentration in (a) and the solid line marks bulk phase separation. (c) Surface phase diagram of $SC_{10}E_2S/AlCl_3$ mixtures with the bulk phase boundary between one and two phase regions marked by the thick grey line. S_1, S_2 and S_m denote surface structures consisting respectively of a normal monolayer plus one, two and several additonal bilayers (NR measurements of these structures are marked by coloured points). Data redrawn from Hui *et al.*[44,46]

monolayer plus one complete bilayer (S_1) and two fringes correspond to a monolayer plus two additional complete bilayers (S_2). In some systems S_3 structures and sometimes multilayer structures are observed. Fig. 4(c) shows the surface phase diagram for $SC_{10}E_2S$–$AlCl_3$, in which the range of $AlCl_3$ concentration over which the S_1 and S_2 structures are formed is large and extends to below the CMC of the pure surfactant. The behaviour of the ST is shown in Fig. 4(b). As expected the addition of small amounts of $AlCl_3$ substantially decreases the ST because the $(SC_{10}E_2S)_3Al$ surfactant has a lower limiting ST and a lower CMC. As further $SC_{10}E_2SNa$ is added the ST gradually returns to the higher value of $SC_{10}E_2SNa$ on its own until it is close to the normal value for $SC_{10}E_2SNa$ above its CMC. The region of positive slope in Fig. 4 corresponding to this change has been interpreted quantitatively by Alargova *et al.* as resulting from the removal of Al^{3+} ions from the bulk solution into micelles.[42,52] Addition of extra $AlCl_3$results in a greater fraction of the Al form of the surfactant at the base of the initial drop in the ST and hence the ST at this point decreases as $[AlCl_3]$ increases and the ST minimum deepens. Depending on the chain lengths of the alkyl and alkoxy groups in the surfactant, precipitation may occur between the initial drop in tension and its subsequent increase. Since precipitation is a proper phase transition the ST will become constant while there is precipitation and such a point is just about reached in Fig. 4(b) at the highest Al^{3+} concentration. Multilayers can form outside the range of precipitation, although the two processes are connected, as shown by the position of the phase boundary marked by a thick line in Fig. 4(c). The occurrence of multilayer structures at the A–W surface has been shown to be linked to the pattern of aggregation in the bulk solution of these systems,[46] the effect of adding higher valency ions being to increase the packing fraction and to favour elongated or eventually lamellar structures.

The surface behaviour changes when the charge is spread from a single ion to an arrangement where the total charge is split into single charges on separate chemical groups, either relatively compact, such as the PO_4^{3-} ion or more widely spaced, as in fully protonated oligoamines such as diethylene triamine[53,54] and spermidine,[55] where the conformation of the charges is flexible, or in melamine[55] and trisodium naphthalene trisulfonate,[56,57] in both of which the charges are fixed in a plane. All the cationics at low pH lower the CMC of SDS, increase the surface excess (NR), and decrease the ST at this lower CMC, similarly to the addition of Al^{3+} described above. Reducing the charge on the amine by increasing the pH usually approximately restores the ST behaviour to its pure value, although the binding of SDS may itself induce some ionization.[58]

The series of oligoanions of which the trisodium naphthalene trisulfonate (POS_3, shown in Fig. 5(a)) is a smaller

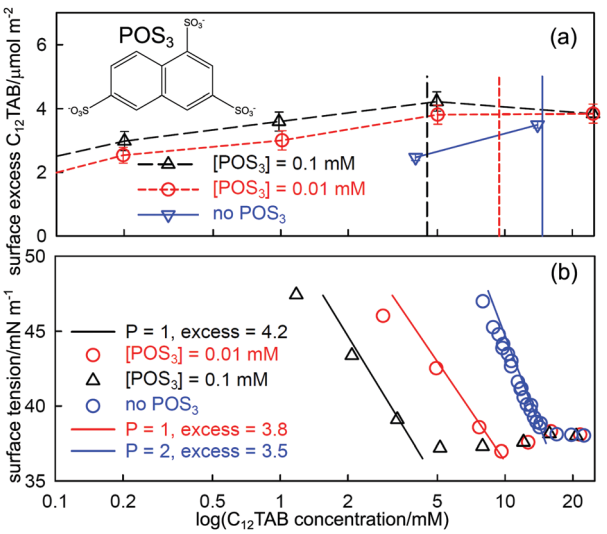

Fig. 5 (a) Surface excesses of $C_{12}TA^+$measured by NR at the A–W interface of $C_{12}TAB$ on its own and with added amounts of 0.01 mM and 0.1 mM POS_3 (trianion structure as shown in (a)), (b) the ST of the same set of solutions with fits of the integrated Gibbs equation using the prefactors and the surface excesses at the measured CMC given in the diagram, and the ST at the plateau. Data redrawn from Jiang *et al.*[57]

representative, are particularly interesting in that the behaviour of mixtures of the oligoions with the cationic C_{12}TAB evolves until it is similar to the behaviour of anionic polymers with C_{12}TAB, which we consider in the next section. The behaviour of the surface excess of C_{12}TAB on its own and in mixtures with low fixed concentrations of 0.01 and 0.1 mM of the acid form of POS_3, all measured using NR, is shown in Fig. 5(a). Fig. 5(b) compares the measured ST of the same solutions with that calculated from the integrated Gibbs equation using the measured surface excess from NR in (a). The Gibbs prefactor P (see eqn (8)) for C_{12}TAB on its own is 2 but, for the solutions with added POS_3 at a fixed concentration, it becomes 1 if the neutral adsorbed species is three $C_{12}TA^+$ and one POS_3 ion (see also discussion in the following section). Thus, although the surface excess of $C_{12}TA^+$ is lower on its own, the magnitude of the slope of the Gibbs plot is greater, as observed. That the Gibbs equation accounts correctly for the ST of the three solutions in Fig. 5 up to the ST plateau shows that the onset of the plateau must be some sort of aggregation. Since no precipitation was observed by Jiang *et al.* for POS_3, although precipitation was observed for the higher members of the series $POS_4$and POS_6,[57] the only possible explanation of the plateau is that it is micellization, just as for Al^{3+} with $SC_{10}E_2S$ in Fig. 4(b). The effect of the POS_3 ion on the CMC and its associated effect on the surface excess and the ST at the CMC then approximately parallel that in Fig. 4(b). Just as in the $SC_{10}E_2S$–Al^{3+}system, the addition of further surfactant gradually solubilizes the POS_3 ion into the bulk solution and its fraction at the surface decreases to zero. This will cause the ST eventually to change to a value closer to that for C_{12}TAB on its own in solution, which is likely to be close to the initial plateau. Although the situation is more complicated than the usual surfactant adsorption, the successful application of the Gibbs equation to the initial drop in ST using NR shows that this must be the onset of aggregation. Menger and Shi[15,56] and more recently Phan *et al.*[33,59] have interpreted conductivity changes in the range above the CMC as a second CMC. However, this is a region where interpretation of the conductivity is complicated by exchange of the counterions POS_3^{3-} and Br^- between solution and micelles and, in any case, the break in conductivity is barely noticeable, as shown in Fig. 9 of Jiang *et al.*[57]

The approximate Gibbs equation for a polyelectrolyte can be written in terms of the counterion X as[61,66]

$$d\sigma = -\Gamma_X RT d\ln c_X f_\pm \approx -\Gamma_X RT d\ln c_X \qquad (9)$$

where the counterions may include both polymer counterions and surfactant ions. In region A the surfactant ion may dominate the surface behaviour but only if the total counterion concentration (surfactant + added electrolyte) is high. In the absence of added electrolyte counterion condensation will usually occur,[67] in which case the activity coefficient $f_\pm$ is small[68] and the gradient of the Gibbs plot is shallow.[61] Thus, even if there is significant adsorption of a polymer and surfactant at the surface the ST will remain approximately constant in region A. This is evidently the case for both systems shown in Fig. 6 where the starting value of the ST for region B is high.

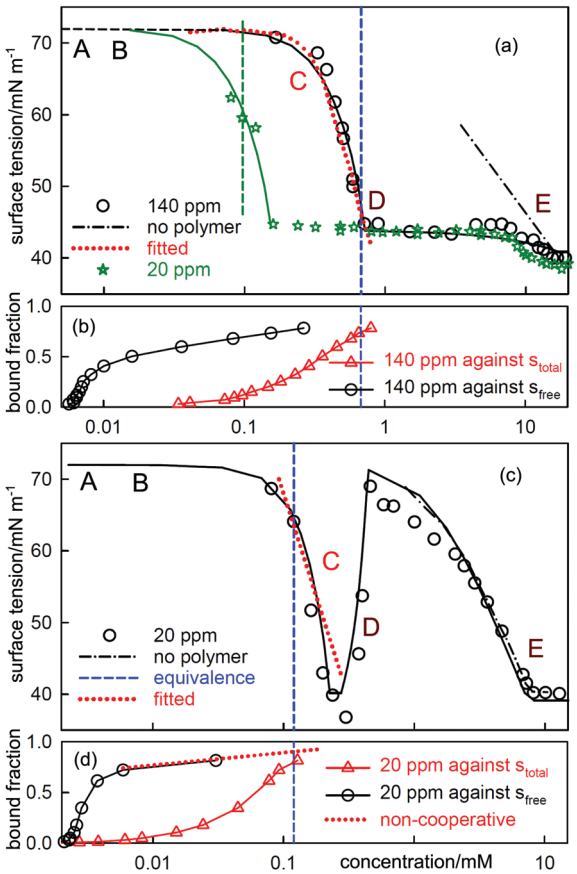

Fig. 6 ST measurements for (a) C_{12}TAB with NaPSS (MW = 18k) at concentrations of 140 ppm and 20 ppm and (c) SDS with 20 ppm PDDA (MW = 100k), and the corresponding independently determined binding isotherms in (b) and (d). The equivalence points are shown as vertical dashed lines. The horizontal axes in (b) and (d) refer to either total or free surfactant as indicated. The red dotted lines are calculated using the Gibbs equation with the observed surface excesses and free surfactant concentrations. The letters ABCDE are explained in the text. The continuous lines through the data are based on the application of a semi-empirical model of Bahramian *et al.*[60] and are drawn primarily to guide the eye. The NR data are redrawn from ref. 61–63 and the binding isotherms redrawn and calculated in terms of total surfactant concentration using ref. 64 and 65.

The concentration of free surfactant, s_{free}, in region B, *i.e.* c_X in eqn (9), varies very little in the cooperative binding range and the ST therefore remains at its high plateau value throughout B, and is almost independent of the behaviour of the surface excess when plotted with respect to s_{total}. Cooperative binding usually changes to non-cooperative binding significantly below charge neutralization so that there is a region C where s_{free} increases rapidly relative to s_{total}. Since there is already significant adsorption in region B (as indicated by NR), this combines with the onset of a sharp increase in s_{free} (or c_X), to give a sharp drop in the ST (region C), which is observed in both systems in Fig. 6. The steep drops in ST can be calculated from the binding curves and the measured surface excesses using the Gibbs equation (eqn (9)), and are shown as red dotted lines in Fig. 6(a) and (c). The calculated drop matches the observed drop in ST even though it is unusually sharp, about four times

greater than for a typical saturated surfactant layer approaching the CMC. Non-cooperative binding is expected to be completed at equivalence, *i.e.* at the onset of formation of the low solubility polymer-surfactant complex. At the formation of such a complex the ST should be constant until sufficient surfactant leads to some further change in the system at point E. The expected plateau does not, however, occur for PDDA and may be interrupted for PSS-C_nTAB, as discussed below.

When electrolyte is present the whole appearance of the ST curve changes. In region A the presence of the background electrolyte prevents counterion condensation, *i.e.* $f_{\pm}$ is closer to unity. The ST behaviour is then determined approximately by the usual equation for a free surfactant with the same solution concentration as the total surfactant.[71] This largely determines the gradient of the plot because the surface excess of surfactant ion is approximately constant. This effect of added electrolyte in region A is seen for both polymer–surfactant systems in Fig. 7. The same behaviour occurs without added electrolyte when the separation of charge in the polymer is too large for counterion condensation to occur, *e.g.* in SDS–polylysine mixtures.[71] The initial and early decrease in ST therefore depends only on s_{total}. A further important difference is that the cooperative binding curve moves to higher concentration on addition of electrolyte, the opposite of the change in CMC of the surfactant.[72] The stage of cooperative binding where s_{free} is almost constant (region B) again leads to a plateau in the ST, but this is now at a low value of the ST. At the end of cooperative binding the gradient of the decrease in the ST should again be much greater for the same reason as in the absence of electrolyte. This is observed for the PSS system, for which the decrease is towards the precipitation plateau. However, in the PDMA system there is an abrupt increase in the ST followed by a decrease that gradually becomes similar to that expected for the free surfactant.

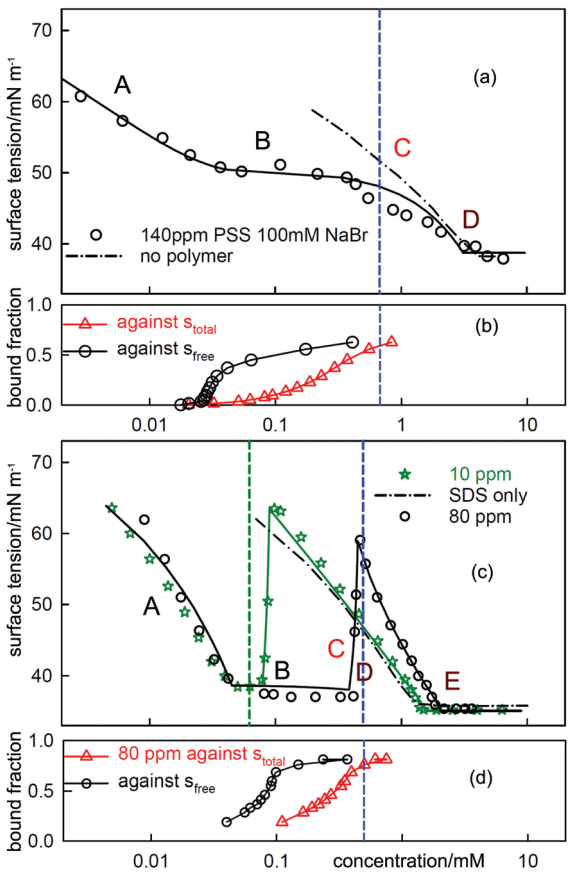

Fig. 7 The equivalent measurements to those in Fig. 6 but with electrolyte, (a) C_{12}TAB with NaPSS (MW = 18k) at a concentration of 140 ppm with 100 mM NaBr and (c) SDS with 10 ppm and 80 PDDA (MW = 100k) with 100 mM NaCl. The NR data are redrawn from ref. 69 and 70 and the binding isotherms redrawn from ref. 64 and 65.

At the start of region D the ST should be dominated by the surface behaviour of the PE-S complex but by the end, when the polyelectrolyte has been fully solubilized, it should be dominated by surfactant. In systems such as PSS-C_{12}TAB the start of region D is the onset of the ST plateau that signals phase separation,[64] but in PDDA-SDS with electrolyte it starts with an ST peak. A peak sometimes also appears at some point along the plateau for PSS-C_nTAB systems.[73,74] As was shown by Staples *et al.* the ST peak in the PDDA-SDS system with electrolyte approximately coincides with precipitation.[70] In the simple situation where both the precipitate and the adsorbed layer have the composition $PS_{1.0}$ the Gibbs equation would require that there is no change in the ST. In that situation the positive ST gradient required for the onset of an ST peak could then only result from depletion, *i.e.* the limiting solubility is too low to sustain the adsorption at its correct equilibrium value. This is a known experimental difficulty when measuring the ST of substances of low solubility,[75] but the true equilibrium ST should not change at the onset of precipitation.

NR gives a result that suggests the cause of this difference between the two systems, which is that the surface species for both PDDA-SDS and PSS-C_{12}TAB are completely different for the two systems and each has a remarkably constant stoichiometry. For PDDA-SDS (in electrolyte) the adsorbed layer consists approximately of two polymer segments to one surfactant, *i.e.* P_2S over regions B, C and D, whereas for PSS-C_nTAB (no added electrolyte) it is PS_2. The approximate constancy of the composition over a wide concentration range suggests that all alternative stoichiometries are not surface active. This is not surprising because at low stoichiometry the surfactants would be too far apart to screen high ST water from air, and at high stoichiometry they would tend to form either a hydrophobic rod or a three dimensional structure of surfactant aggregates, neither of which is likely to be surface active at the A–W interface. For a fixed surface stoichiometry, PS_θ, adsorption will generally be optimized when the mean activity of PS_θ in the solution is the same as in the complex, *i.e.* when the solution is also approximately PS_θ. However, when precipitation of the 1 : 1 complex occurs it has the effect of displacing the solution equilibria strongly towards the composition of the precipitate. Precipitation of a 1 : 1 precipitate in the PDDA-SDS system should therefore cause a decrease in the mean solution activity of complex $PS_{0.5}$. If this decrease occurs in region C, where s_{free} changes unusually sharply with s_{total}, it is possible that as well

as an initial steep decrease in ST, precipitation may cause this to reverse and lead to corresponding sharp increase in ST. Indeed, the ST behaviour for PDDA-SDS without added electrolyte suggests just such a reversal between sharp negative gradient and sharp positive gradient. A decrease in the mean activity of the $PS_{0.5}$ complex should also reduce its adsorption but this would not usually be a large effect. Some reduction in adsorption in the precipitation region was observed by Staples *et al.* That the corresponding effect does not occur for the PSS-C_{12}TAB system is then simply that the activity of the surface complex, now PS_2, is not affected at the onset of precipitation of the 1 : 1 complex.

When the surface active complex has a greater molar content of surfactant as in the PS_2 complex of the PSS-C_{12}TAB system its mean activity will not be reduced by precipitation of 1 : 1 PS because PS can equilibrate with further S to maintain the bulk mean activity of any PS_θ complex with $\theta > 1$. Thus, no ST peak should occur for PSS-C_nTAB provided that the precipitate remains the 1 : 1 complex. The ternary phase diagram determined for NaPSS with C_{16}TACl has been determined by Sitar *et al.*[76] and by Nause *et al.*[77] Although these studies were not done in the extremely dilute conditions of the surface experiments, it can be concluded that the precipitate develops along the plateau into a hexagonal phase incorporating up to about 15 molecules of extra surfactant[76] close to the redissolution limit. The length of the plateau in the surface experiments also shows that the onset of region E, *i.e.* complete redissolution, is reached at a similar composition. Towards the end of the plateau, at a θ value >2 a relatively sharp peak is sometimes observed for C_{12}TAB and C_{14}TAB,[73,74] and more definitely for C_{16}TAB.[73] One of the conditions that causes the peak in the PDDA-SDS system is that a precipitate of higher stoichiometry than PS_2 reduces the solution activity of the PS_2 complex, and that can apply to the PSS-C_nTAB system at a correspondingly higher concentration. However, the extra sharpness arising from the cooperativity of the binding in PDDA-SDS is not present. This and the erratic appearance of the peak indicate that in the PSS-C_nTAB system the peak is a result of either depletion or non-equilibrium.

2.6 Association in solution

The main aggregation of surfactants in solution is usually micellization at the CMC. Micellization is not a true phase change and it is generally assumed to occur over a narrow but finite range of concentration,[18,38] *i.e.* micelles start to form just below the CMC and this is often referred to as premicellization. Such a process would be expected to be assisted by traces of impurity and it is then not surprising that it is difficult to establish unambigously whether it occurs in pure systems.[78] However, surfactants with more complicated hydrophobic structures may dimerize or form limited small aggregates at concentrations well below the CMC, which we refer to here as dimerization or oligomerization, reserving the term "premicellization" for aggregation very close to the CMC. Gemini surfactants consist of two ionic surfactant groupings with their head groups attached by a link of varying length. The presence of two

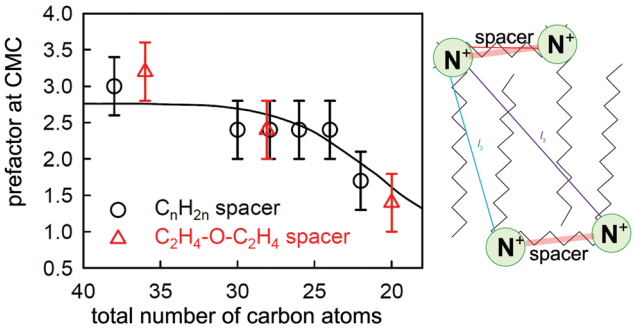

Fig. 8 The experimentally determined prefactor P in the Gibbs equation at the CMC (points) of $C_nNMe_2C_6NMe_2C_nBr_2$ (black circles) and $C_nNMe_2C_2$-O-$C_2NMe_2C_nBr_2$ (red triangles) and a calculated value (line) based on the structure shown alongside and a model described in the text. The two points at 28 carbons have been laterally displaced from each other for clarity. Key distances between charged groups are marked in the structure shown. Figure redrawn from Li *et al.*[80]

hydrocarbon chains is expected to favour dimerization and the presence of two head groups is expected to favour ion pairing in the bulk solution, as suggested by a model originally shown by Song and Rosen,[79] and here shown in a more detailed form in Fig. 8. As well as being a possible conformation for a bulk dimer this model has relatively short distances between the charged groups, which would cause it to bind counterions.

For a divalent gemini ion, the Gibbs equation can be written as

$$-\mathrm{d}\sigma = -P\Gamma RT d\ln m_{\pm}f_{\pm} \qquad (10)$$

where P is the number of ions per adsorbed neutral unit, *i.e.* 3 for a fully dissociated gemini, Γ is the surface excess of the neutral gemini, and $f_{\pm}$ and $m_{\pm}$ are respectively the mean activity coefficient and mean concentration of the adsorbed species in the bulk solution.[21] Values of P different from 3 and/or interactions that cause $f_{\pm}$ to be different from 1 will lead to inconsistencies between the surface excesses determined by ST measurements using the Gibbs plot of eqn (10) with $f_{\pm} = 1$ and those determined directly by NR, which do not require the use of the Gibbs equation.

The series of geminis $C_nNMe_2C_mNMe_2C_nBr_2$, where C_n and C_m are hydrocarbon chains and the N are quaternary charged links, has been extensively investigated. ST and NR showed that for values of m of 3, 4, 6 and n = 12 the limiting value of P is close to 2 for all four compounds,[81] *i.e.* these gemini are mostly associated in solution in a way that makes P in eqn (10) equal to about 2 at the CMC instead of the expected value of 3. In earlier ST measurements on the same series Alami *et al.*[82] had assumed that P was 3 and their studies on the same series of compounds using conductivity indicated no association.[83–85] However, although conductivity is known to be sensitive to both ion pairing and to dimerization in geminis, these processes have opposite effects, which means that they tend to cancel, which further suggests that more than just an approximate cancellation may be required to explain the conductivity data, see *e.g.* ref. 86.

More recent NR measurements have been made on two sets of geminis using spacers of either C_6H_{12} or $C_2H_4OC_2H_4$ as link, with a range of chain lengths of the two side chains.[80] The value of P required to bring the limiting ST and NR measurements at the CMC into agreement is plotted against the total number of carbon atoms for these compounds in Fig. 8, and it varies from 3 for the longer chains to less than 2 for the shorter ones. This can only result from effects of dimerization and/or ion binding on either the prefactor P and/or the mean activity coefficient $f_{\pm}$ of the neutral GBr_2 that adsorbs at the surface. Thus, the unambiguous result from the observed ratio from the two relatively simple measurements of NR and ST, without any detailed analysis, again shows that (i) there is some sort of association of the gemini ions in the bulk solution, (ii) this varies between different geminis, and (iii) it persists to concentrations significantly below the CMC. Li *et al.* devised a model to interpret this behaviour, which involved an empirical constant for dimerization, a known constant for ion binding in bolaform surfactants,[87] and geometrical and statistical considerations based on the structure shown in Fig. 8 and the Gibbs equation, and were able to account for the general behaviour of the change in P at the CMC as shown in Fig. 8. However, the model did not account well for the variation of P with concentration for several of the geminis studied. Nevertheless, despite its limitations, it demonstrates covincingly that the association in the bulk solution of geminis involves both dimerization and ion pairing.

Examination of ST measurements on other series of geminis in the light of the NR/ST results described above indicates that the strength of dimerization and ion binding vary substantially according to head group and spacer structure. If the interactions are strong, some clear and interesting features appear in the ST curves on their own. The first of these concerns the CMC and the limiting ST at the CMC and was identified by Menger and Littau[88] and analysed quantitatively by Rosen *et al.*[79,89] The dimer drawn in Fig. 8 would obviously not be surface active and would not be a stable entity to exist in a micelle. Thus, if dimerization is significant the concentration of monomers is reduced with the effect that the overall concentration needed to attain micellization is reduced and the CMC shifts to a higher concentration, with a higher limiting ST, and this is indeed observed. Song and Rosen further concluded that geminis with a more flexible spacer were more likely to aggregate, in agreement with the observation of Li *et al.*[81] that, in the series they studied, only the spacer containing the xylyl group was fully dissociated at the CMC. More recently, Cai *et al.* have explored a series of geminis with two bulky pyrrolidone head groups and an alkyl chain spacer.[90] As the spacer is increased in length, the CMC and the limiting ST both increase, as analysed by Song and Rosen. However, what is more interesting is the behaviour of Cai *et al.*'s long spacer surfactants (LSS) at low concentrations. The greater carbon content of the LSS should make them unusually surface active at low concentrations so that they have an unusually long range of high surface activity, *i.e.* the surface excess should remain relatively constant over an unusually wide range of concentration. In the LSS of Cai *et al.* this long range makes it possible to observe a transition resulting from a change in P, *i.e.* the *equilibrium* Gibbs plot becomes steeper at low concentrations. Taking the simple model of Li *et al.*[80] and assuming no change in the area per molecule between Cai *et al.*'s $C_{12}C_{16}C_{12}$PB at its measured CMC in NaCl and that at the low concentration break in the absence of salt, the change in P should lead to apparent areas per molecule with a ratio of 1 : 3, which is close to the observed values of 1.70 : 3.78. This is consistent with the general features of the model of Li *et al.* However, that dimerization and ion binding should give rise to an apparently sharp break in the ST does not mean that this should be considered as a phase change analogous to the CMC. Chemical equilibria of this sort are normally plotted on a linear concentration scale. The use of log c and the significant error bars in a Gibbs plot may simply give an illusion of sharpness. Cai *et al.* also showed that the conductivity of these geminis followed the pattern expected for significant aggregation as the spacer length increased. This and the apparent sharpness of the break almost certainly results from the stronger aggregation and counterion binding in these pyrrolidone geminis compared with the simpler compounds studied by Li *et al.*

2.7 Dissociation in solution

Just as association in solution can have unexpected effects on the application of the Gibbs equation, as discussed above, so can unexpected dissociation. This is potentially a significant problem for polymers that are subject to either the incorporation of occasional charged groups *via* impurity monomer residues or *via* hydrolysis of a small fraction of residues. The presence of charged groups changes the P factor in the Gibbs equation, which can have a large effect on the ST of their solutions, even at a very low level. Polyacrylamide is an example of such a polymer and it is known to be susceptible to a low level of hydrolysis that leads to a fraction of carboxylic acid residues, and partial hydrolysis is often used deliberately to improve the solubility of commercial hydrophobically modified polyacrylamides.[91]

Zhang *et al.* prepared a set of hydrophobically modified PAM with 0.5, 1 and 2% of the residues modified by the attachment of perdeuterated $C_{12}D_{25}$ hydrophobic groups.[92] The structure and composition of layers adsorbed at the A–W interface was determined by NR on samples in null reflecting water and in D_2O. This made it possible to determine directly the area per added hydrophobic unit by NR, and the corresponding values of the surface excess per hydrophobic segment are shown in Fig. 9(a) for three polymer samples with different fractions of hydrophobe. The adsorption is strongest for the sample of greatest hydrophobicity (1 : 50) and the surface excess of all three samples increases approximately linearly with log$c$. The ST results, shown in Fig. 9(b), also show a systematic pattern of behaviour that is qualitatively consistent with the NR measurements in that the ST has a negative slope that increases with concentration and hydrophobicity as would be expected. However, the magnitude of the slope is unexpectedly high for a neutral polymer.

The steepness of the slopes in Fig. 9(b) can be explained if a low level of hydrolysis of acrylamide to acrylic acid groups

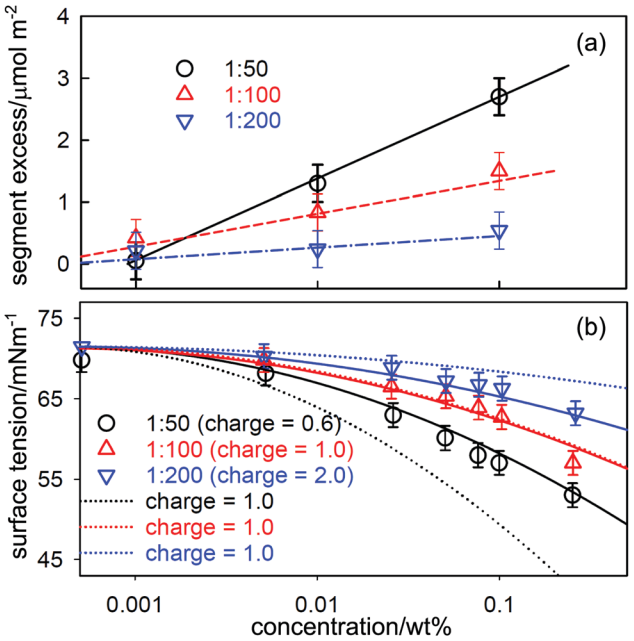

Fig. 9 (a) Surface excess, Γ, per hydrophobic segment for a hydrophobically modified PAM containing 1 hydrophobic group per 50, 100 and 200 residues as a function of concentration. The linear variation of Γ with log c shown in (a) was used in the Gibbs equation to calculate the surface tension behaviour in (b) using two assumptions. In the first (continuous lines) the charge on the PAM backbone was taken to be 1 per 100 backbone units making the charge per hydrophobic unit respectively 0.5, 1 or 2 for 2, 1 and 0.5 mol% HMPAM. In the second assumption (dotted lines) the charge along the backbone was taken to be one per hydrophobic unit. Reprinted by permission from Zhang *et al.*[92]

occurs during the polymerization. This converts the polymer into a weak polyelectrolyte, for which the Gibbs equation can be written as[61,66]

$$d\sigma = -\Gamma_X RT d\ln c_X f_\pm \approx -\Gamma_X RT d\ln c_X \qquad (11)$$

where X represents a charged unit. For example, if the mean charge is one per 100 backbone units Γ_X would be identical with the surface excess *per hydrophobic unit* for the 1 mol% HMPAM, but half and twice the surface excess per hydrophobic unit for the 2 mol% and 0.5 mol% HMPAMs respectively. Fig. 9(b) shows fits of the Gibbs equation in the form of eqn (11) to the values of coverage calculated from slopes in (Fig. 9(a)) based on the assumption that the average charge on the PAM is 1 per 100 backbone residues. Although the use of eqn (11) makes a number of assumptions, including complete dissociation and ideal behaviour, neither of which is appropriate for most polyelectrolyte systems, the fit is remarkably good. The surprisingly steep slope then arises because it is the loss of entropy of the several ions per polymer that dominates the changes in the ST.

3 Mixing at the air–water surface and in micelles

We have already shown that NR can be used to study the surface composition of mixtures of surfactants above and below the critical micelle concentration (CMC.) The absence of sublayer structure in most micellar systems also shows that there is no interaction between the monolayer and the micelles in such systems and therefore the surface interactions that determine the optimum composition of the monolayer do not change at the CMC. Thus any changes in the surface composition above the CMC can result only from changes in the bulk monomer activities on micellization or, more simply, only from changes in the monomer concentrations above the CMC, which themselves are largely determined by the composition of the micelles. Thus, measurement of the variation of the surface composition offers a means of studying the interactions between surfactants not only in the monolayer but also in the micelles. Since the geometry of self-assembly in micelles and flat interfaces is different, differences in the interactions can also be expected between the two structures. This is an area that is uniquely accessible to NR and the results in this section are a survey of the progress that has so far been made. Although not strictly necessary for the analysis of some of the results presented, the independent technique of neutron small angle scattering (SANS) can also make use of isotopic substitution to measure the composition of mixed micelles. However, in that SANS is also affected by the shape and size of the micelle, it is not in principle as accurate a method as NR for the determination of composition.

An expression for calculating the monomer and micellar composition of a ideal binary mixture of surfactants at concentrations above the CMC was first given by Clint.[93] The calculation was extended to the micellization of non-ideally mixing surfactants by Rubingh, who used the regular solution model to account for the non-ideality.[94] In this model the excess free energy of mixing in the micelle is

$$\Delta G_E = BRTx_1x_2 \qquad (12)$$

where B is a constant and $x_i$are the mole fractions of the two surfactants in the micelle. This also assumes that the surfactants behave as though they are nonionic, *i.e.* that there are no complications from dissociation into ions. Most practical surfactant formulations involve more than two surfactants and Holland and Rubingh extended the regular solution model to more than two components. For example, a three component system is characterized by three contributions to the excess free energy with interaction constants, B_{12}, B_{23} and B_{31}.[95,96] Ingram later argued that this mixing model for micelles, usually described as the pseudophase approximation (PPA), can also be used to relate the composition of mixed surfactant layers at a defined surface pressure to their solution composition.[97] Thus, above the CMC, where the surface pressure is often approximately constant, the monomer concentrations can be calculated by fitting the values of the CMC to a value of B_m for the interaction in the micelles, and the result is then used to calculate the surface composition with a value of B_s for the surface interaction, where B_s is not necessarily the same as B_m.

The experimental limitations of the early work on surfactant mixtures were (i) that the only means of determining a fractional surface excess was to apply the Gibbs equation to one

component at a time while maintaining the other(s) at a fixed concentration,[19] (ii) that surface excesses could not be determined above the CMC, and (iii) there was no method for determining micellar composition. Nevertheless, it was shown that the CMC variation with composition could be explained in terms of the regular solution model and that the variation of the surface with the bulk composition could sometimes also be explained.[98] The main difficulties from a theoretical point of view have been how to handle the dissociation of ionic surfactants in this framework, *e.g.* ref. 99 and 100, and that fitted values of the interaction parameter often vary with composition, indicating that the regular solution model is not being obeyed, *e.g.* ref. 101. This is not unexpected for the surface because the natural hexagonal packing in a plane does not favour the 1 : 1 composition required by eqn (12) (see, *e.g.* ref. 102).

As already shown, NR can give direct access to the surface excess of a surfactant at the A–W interface, irrespective of either the presence of other surfactants at the surface or the state of aggregation in the underlying solution. For mixtures above the CMC the activities/concentrations of the monomers determine the surface composition *via* the adsorption isotherm and hence must also be determined. In addition, small angle neutron scattering (SANS) is able to determine the composition of mixed micelles using selective deuteration, similarly to NR, but usually reversed, *i.e.* the surfactant of interest is usually protonated with the remaining surfactants perdeuterated and D_2O is used instead of null reflecting water.

The theoretical model used to describe mixing in either micelles or at the A–W interface derives from the Butler equation,[103] which has recently been shown to conform with the Gibbs equation.[104,105] The additional key approximation is then that the adsorbed layer consists only of surfactants, *i.e.* it contains no water and no empty space. For a binary mixture of uncharged surfactants at a fixed surface pressure, π,

$$\frac{\alpha_1}{f_1^s c_1^\pi} + \frac{\alpha_2}{f_2^s c_2^\pi} = \frac{1}{c_{\text{mix}}^\pi} \tag{13}$$

where c_i^π are the concentrations at which a solution of component i or the mixture has a particular surface pressure, and f_i^s are the activity coefficients of the two components in the adsorbed layer (the bulk activity coefficients are assumed to be unity), and α_i are the mole fractions in solution. In the regular solution approximation, eqn (12), the activity coefficient of a component in the layer is given by

$$\ln f_i^s = B_s x_j^2 \tag{14}$$

where x_i are the mole fractions of surfactant in the layer. This expression for f_i^s can be substituted into eqn (13), which then has to be solved by iteration. A version that is easier to solve when higher free energy terms are included is[106,107]

$$\ln\left(\frac{f_1^s}{f_2^s}\right) = B_s(x_1 - x_2) = \ln\left[\frac{x_1 c_1^\pi \alpha_2}{x_2 c_2^\pi \alpha_1}\right] \tag{15}$$

and then the following equation,

$$B_s(x_1 - x_2) = \ln\left[\frac{x_1 c_1^\pi \alpha_2}{x_2 c_2^\pi \alpha_1}\right] \tag{16}$$

is solved by iteration using a suitable iteration method.[108]

The restriction to the regular solution model is likely to be physically unrealistic for many adsorbed mixed layers. Ways of removing this restriction have tended to focus on dissociation or the electrostatic interaction when an ionic surfactant is part of the mixture, *e.g.* Ref. 99 However, the well established method for liquid mixtures is to expand the free energy of eqn (12) as the series

$$G_{\text{excess}} = RTx_1x_2[B_s + C_s\,(x_1 - x_2) + D_s\,(x_1 - x_2)^2 + \ldots] \tag{17}$$

where B_s, C_s and D_s are constants appropriate to the surface layer.[106,109–111] This has the advantage that it conforms with the requirement that a true phase should obey the Gibbs–Duhem equation, *i.e.* it applies as a consequence of the pseudophase approximation, and that it is relatively easy to add to eqn (16) for iterative solution. The activity coefficients now become[110,111]

$$\ln f_1 = B_s x_2^2 + x_2^2\,(3 - 4x_2)C_s + x_2^2\,(5 - 16x_2 + 12x_2^2)D_s \tag{18}$$

with a parallel expression for f_2 except that the sign changes for the C_s term. The simultaneous solution of eqn (16) can still be done accurately by iteration using the sector method unless the interactions become so strong that they lead to phase separation.

The calculation of the mixed CMC uses exactly the same equations as the surface layer at constant pressure except that the c^π are replaced throughout the above equations by c^μ, the CMC, and B_s, C_s and D_s are replaced by the corresponding B_m, C_m and D_m. However, the more wide ranging set of measurements is of the surface coverage above the CMC and their calculation from the pseudophase model is more complicated. It requires two steps, one to calculate the monomer concentrations and the second to use the monomer concentrations to calculate the adsorption. The second of these steps is exactly the same as for below the CMC, *i.e.* as described above, but the first step is different.

The monomer concentration above the CMC for a binary mixture, c_i^m, is[94]

$$x_i = \frac{c_i^m}{f_i c_i^\mu} \tag{19}$$

where the activity coefficient of the monomer in solution is again assumed to be unity. Mass balance requires

$$x_1 = \frac{\alpha_1 c - f_1 x_1 c_1^m}{c - f_1 x_1 c_1^m - f_2 x_2 c_2^m} \tag{20}$$

where c is the concentration, and this gives the following equation suitable for iteration

$$F = Ax_1^2 + (c - A)\,x_1 - \alpha_1 c \tag{21}$$

where

$$A = f_2 c_2^m - f_1 c_1^m \quad (22)$$

and the activity coefficients are as given in eqn (18) with the parameters being those for mixing in the micelle. Eqn (20) is a quadratic equation and there is then the choice of solving either the quadratic or its root by iteration. We have found that the simple sector method of iteration works satisfactorily on the quadratic, although it is important to monitor the iteration to ensure that it is selecting the physically sensible root. The monomer fractions calculated from eqn (20) are the α values for calculating the surface adsorption using the same interaction parameters as apply below the CMC and using eqn (15) and (16).

The surface equations given so far apply at constant surface pressure π. In the case of measurements above the CMC, although the surface pressure is often constant with the bulk concentration, it can be quite different between the pure components and between the pure components and the mixture. However, B_s depends on the surface pressure because the values of c_i^π depend on π through

$$c_i^\pi = c_i^{\pi=0} \exp\left(\frac{\pi\omega_i}{RT}\right) \quad (23)$$

where ω_i is the molecular area of surfactant i and $c_i^{\pi=0}$ is a measure of its binding to the surface at zero pressure.[104,109] Values of c^π are best obtained by interpolation of the ST curves using fitted quadratics in lncat the highest possible surface pressure in each case, *i.e.* close to the limiting ST at the CMC of the less surface active component. Unless the difference in limiting partial molar areas is large the surface pressure correction is small for measurements above the CMC. However, the effect can become large below the CMC if a wide range of ST is being explored and/or if there is a substantial difference in the values of ω_i. This is expected to be the case for a typical polymer where polydispersity means that some components have a very much smaller ω_i than others.

The extension of either the regular solution or the more general expansion of eqn (17) to more than two components is straightforward in principle. However, the expressions for the activity coefficients need to be evaluated following the procedure of Redlich and Kister[106] and the iterations have to be followed particularly carefully when more than two components are used. Details of extensions to three and to five components have been given by Liley *et al.*[112,113] A further difficulty is how to display the results. This was done by Liley *et al.* using triangular coordinates for the three component system, but the five component system had to be plotted as binary pairs. It might be thought that the analysis of such complicated mixtures is not worth the extra difficulty. However, many formulations contain more than five surfactants and such analyses are therefore of significant practical importance.

3.1 Binary mixtures close to ideal mixing

For binary mixtures of nonionic surfactants, or pairs of surfactants with similar structures, the mixing is expected to be close to ideal.[19,98,115] On the basis of CMC data alone it is difficult to determine the small variations from ideality and their impact upon the evolution of the surface composition with solution concentration and composition. This is illustrated by a recent study of the adsorption and self-assembly in two alkyl α-sulfoester surfactants, which we abbreviate to C_nMES in the case of the methyl ester. Xu *et al.*[114] characterised the surface and micelle mixing in the eutectic mixture of C_{16}MES and C_{18}MES, in which the only difference is the alkyl chain length and therefore the mixing should be close to ideal. The variation in surface composition with solution concentration for the eutectic mixture at 65 : 35 mole ratio was measured by NR and is shown in Fig. 10. The impact of the onset of micellisation is clearly seen in the abrupt change in the surface composition with increasing surfactant concentration. Below the CMC the surface composition is constant and is dominated by the more surface active component, C_{18}MES. Above the CMC the surface composition is close to the solution composition, but in the concentration range studied it has not yet evolved towards the solution composition of 65 : 35 mole ratio C_{16}MES : C_{18}MES. The calculated lines in Fig. 10 are PPA calculations for a repulsive interaction both at the surface and in the micelle with $B_s = 1.5$ and $B_m = 1.4$ (units of RT), and the higher cubic or quartic contributions to the excess free energy of mixing are zero. Hence the regular solution approximation is adequate in this case. The derived interaction parameters are also consistent with the measured variation in the micelle composition by Xu *et al.*[114] Overall, the data for the eutectic C_{16}MES/C_{18}MES mixture shows two distinct features. The surface composition above the CMC tends towards the solution composition, but below the CMC it is constant and rich in the more surface active component. Although the micelle composition must tend towards the solution compositions, as observed by Xu *et al.*, in this case the surface has a different equilibrium composition because it is now in equilibrium with the free monomer composition in solution, which is different from the overall solution composition. Although the surface composition below the CMC may be constant, as it often is, this is not a constraint

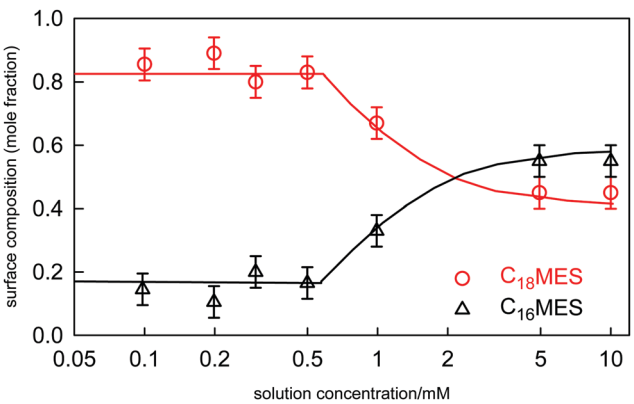

Fig. 10 Variation in surface composition with solution composition for the 65 : 35 mole ratio eutectic mixture of C_{16}MES/C_{18}MES. The lines are model calculations using the PPA with the parameters given in the text. Redrawn from Xu *et al.*[114]

in that it will depend upon the relative surface activities of the different components of the mixture. A later example shows marked deviations from both of these trends for the surface of mixtures of the nonionic alkyl ethoxylates $C_{12}E_3/C_{12}E_8$.

In a related and complementary study Wang *et al.*[116] explored the impact of changing the headgroup structure of C_nMES by means of changes in the ester group on their mixing with other α-sulfo-ester surfactants. NR measurements for the methyl ester, C_{14}MES, mixed with the ethyl ester, C_{14}EES, and propyl ester, C_{14}PES, surfactants showed that the surface adsorption was dominated increasingly by the more surface active component. Analysis of the mixing properties as a function of composition at a fixed concentration above the CMC showed that the surface mixing was close to ideal. However subtle variations and departures from ideal mixing still occur and were characterised using the PPA approach. The C_{14}MES/C_{14}EES mixture was weakly repulsive and close to a regular solution description, with B_s = 0.2, C_s = 0.0, and D_s = 0.0. The interaction between the two surfactants in the C_{14}MES/C_{14}PES mixture was stronger and weakly attractive (with B_s = −0.2, C_s = 0.4), and also unsymmetrical with respect to the surface composition. These small changes imply that changes in the packing associated with the two different mixtures may be quite subtle. They also suggest that the propyl ester group can pack more effectively with the methyl ester group so as to reduce the headgroup interaction and promote greater counterion binding.

Penfold *et al.*[117,118] determined the surface mixing for the nonionic surfactant mixtures of $C_{12}E_3/C_{12}E_8$ by NR. Although the two surfactants have quite different packing requirements with saturation areas per molecule of 30 and 60 Å^2 respectively, they have relatively close CMC values. Following the work of Rosen and Hua,[98] who reported that the micelle and surface mixing was close to ideal, NR measurements were made from below the CMC to about 100 × CMC(mixed) for two different solution compositions with 50 : 50 and 30 : 70 mole ratios, as shown in Fig. 11. The variations in surface composition in Fig. 11 show three striking features, (i) there is an abrupt change in the variation in composition at the CMC due to the onset of micellisation, (ii) the surface composition at concentrations as high as 100 × CMC is significantly different to the solution composition, and (iii) below the CMC the surface composition varies strongly with concentration. Although the PPA analysis[20] of the micelle data and the CMC variation, indicate a small synergistic interaction with B_m = −0.3, the surface interaction is different. The surface interaction is slightly repulsive and asymmetrical, with B_s = 0.8 and C_s = 1.2. This suggests that the repulsive interaction results from the frustration or steric hindrance in packing the different EO groups, E_3 and E_8, at the interface; whereas in the micelle the packing constraints are more relaxed. The frustration results in changes in the structure of the mixed layer compared with the pure components.[118] The alkyl chain distributions of each surfactant were more extended in the mixture. The E_3 group was less hydrated and the E_8 group more hydrated and less extended on mixing. The marked variations below the CMC result from significantly different variations in the surface activity of the two components below the CMC. This occurs here because the two components have different limiting surface areas, STs, and different ST variations with concentration, resulting in a crossover in the surface activity at low concentrations. The NR results show a rich pattern of variation for a system so relatively close to ideal mixing and which was not previously evident. Furthermore the PPA analysis closely captures the main features and trends.

In a study of the adsorption at the air–water interface of a quinary biosurfactant-surfactant mixture Liley *et al.*[113] characterised the several associated binary pairs with NR, of which one was a mixture of the biosurfactants R1 (L-rhamnosyl-β-hydroxydecanoyl-β-hydroxydecanoyl) and R2 (L-rhamnosyl-L-rhamnosyl-β-hydroxydecanoyl-β-hydroxydecanoyl), which provides an interesting complement and contrast to the nonionic mixtures discussed above. The biosurfactants have the same alkyl chain structure, but R2 has a bulkier di-rhamnose headgroup. Recent studies indicate that they are only weakly ionic. The change in the headgroup structure from mono- to

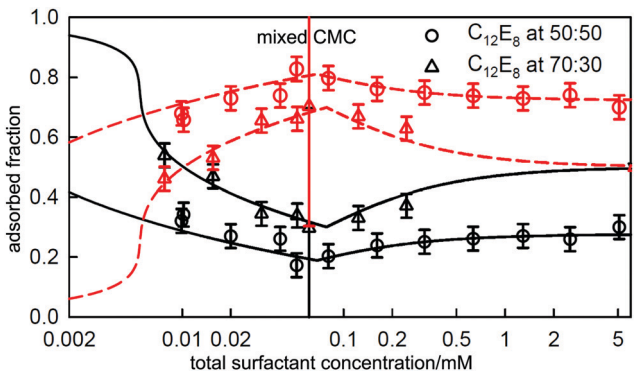

Fig. 11 Variation in surface composition with solution composition for $C_{12}E_3$: $C_{12}E_8$ at 50 : 50 and 30 : 70 mole ratios. The lines are PPA calculations for B_m = −0.3, B_s = 0.8 and C_s = 1.2. Redrawn from ref. 20.

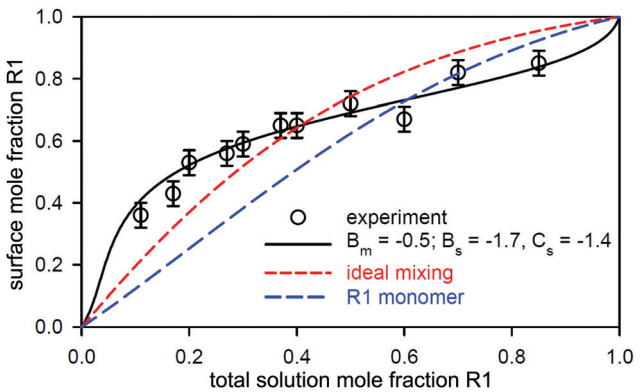

Fig. 12 Variation in surface composition with solution composition for a 1 mM R1/R2 mixture. The black line is the best PPA description for the parameters shown (in units of *RT*), ideal surface mixing is shown as a short dashed red line, and the long dashed blue line is the associated monomer composition. Redrawn from Liley *et al.*[113]

di-rhamnose results in an increased packing constraint at the interface, in which the saturation area/molecule increases from about 60 to about 90 Å^2.[119] NR measurements on the surface as a function of solution composition at a fixed concentration above the CMC show a marked departure from ideal mixing. Thus, although the micelle mixing parameters indicate only a slight departure from ideal mixing with $B_m = -0.5$, the parameters for the surface indicate a stronger asymmetric and synergistic interaction with $B_s = -1.7$ and $C_s = -1.4$. The latter gives rise to a minimum excess free energy of mixing, G_E, which increases from $-0.13RT$ for the micelle to $-0.48RT$ for the surface. The minimum in G_E for the R1/R2 mixing occurs at a 2 : 1 R1 : R2 stoichiometry, and the stronger synergy in the interaction indicates an improved packing at the interface on mixing compared with the $C_{12}E_3/C_{12}E_8$ mixture above. The implications for the quinary mixture involving R1 and R2 are discussed below.

The important theme of the nature of the mixing of biosurfactants with conventional surfactants was continued in a recent study involving a rather different biosurfactant, the saponin, escin. Tucker *et al.*[120] used NR to study the mixing of escin with the nonionic surfactants $C_{12}E_5$ and $C_{12}E_8$ at the air–water interface. Here the NR measurements are more challenging because only the conventional surfactants can be readily deuterium labelled, but it was still possible to determine the surface composition because the scattering length of escin is just sufficiently large enough without deuteration. Escin is only weakly ionic, so that mixing would be expected to be close to ideal. However saponins have a rather different molecular structure from conventional surfactants, with a triterpenoid hydrophobic region and a hydrophilic portion consisting of saccharide groups, and the nature of their mixing with more conventional surfactants was unknown. The CMC variations with $C_{12}E_5$ and $C_{12}E_8$ already indicate an important difference, and it is evident that there is a transition from a weakly to a strongly attractive interaction. The surface mixing was studied at a fixed concentration as a function of solution composition, and at a variable composition with increasing concentration, as shown for escin/$C_{12}E_8$ in Fig. 13.

Fluorocarbon based surfactants offer different opportunities and advantages in some applications over their hydrocarbon equivalents and the mixing of fluorocarbon/hydrocarbon surfactants show some interesting differences because they are characterised predominantly by repulsive interactions. Jackson *et al.*[107] used ST and NR to study the mixing of several partially fluorinated surfactants, *e.g.* $C_4F_9C_{11}H_{22}$TAB with C_{16}TAB and $C_8F_{17}C_6H_{12}$TAB with C_{18}TAB. The mixing was highly asymmetrical and required the quadratic, cubic and quartic terms in the PPA analysis. The mixing properties were quite different at low and high hydrocarbon mole fractions. At low hydrocarbon mole fractions the mixing was close to ideal and repulsive, with the minimum $\Delta G_E \approx 0.2$ to $0.3RT$ at higher mole fractions. Complementary structural measurements, which provided access to the distribution of the different surfactant fragments at the surface, provided an important insight to those changes. At low volume fractions the ideal behaviour results from a balance between the energy gain associated with a reduced immersion of the fluorocarbon chain due to the presence of the hydrocarbon chain, and a loss from increased fluorocarbon/hydrocarbon repulsion. At the higher hydrocarbon volume fractions there is no space for further screening and the increasing fluorocarbon/hydrocarbon repulsion leads to the overall repulsive interaction.

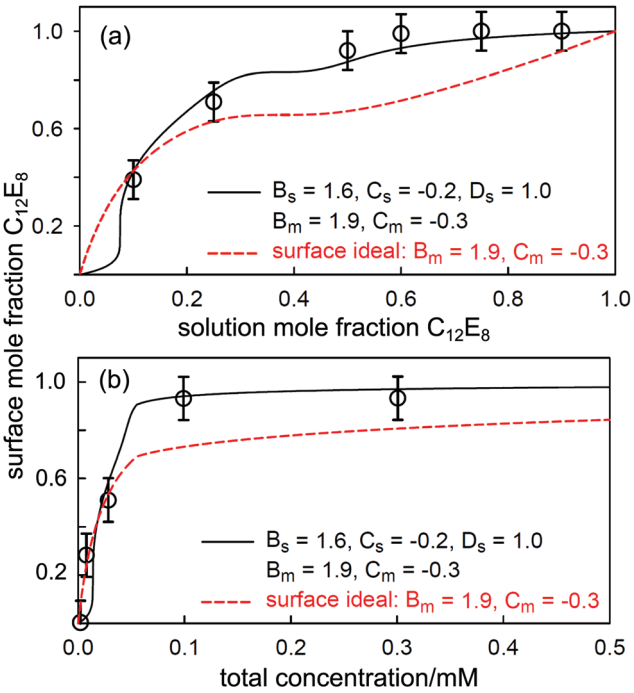

Fig. 13 (a) Variation in surface composition with solution composition at a solution concentration of 0.3 mM for escin/$C_{12}E_8$, (b) variation in surface composition with total surfactant concentration for 0.09 mM escin in $C_{12}E_8$ solutions of varying concentration. The continuous lines are PPA calculations with non-ideal micellization and non-ideal surface mixing and the dashed lines are for non-ideal micellization and ideal surface mixing. Redrawn from Tucker *et al.*[120]

Although in all of these examples in this section the departure from ideal mixing is relatively modest, the ability to characterise the evolution in the surface composition over a wide range of system parameters (mainly composition and concentration) provides the opportunity to probe in some detail the thermodynamics of mixing. It gives some detailed insights into the major factors affecting the mixing behaviour, and demonstrates the applicability of the PPA for such systems. It also illustrates the potential for correlating structural changes in the surface layer directly with the mixing properties.

3.2 Binary ionic/nonionic mixtures

SDS/nonionic surfactant mixtures are representative model systems for many of the mixed surfactant formulations used in home and personal care products and surfactant based formulations in other different product sectors. Penfold *et al.*[121,122] used NR and SANS to investigate the mixing of SDS with a range of different nonionic surfactants, $C_{12}E_3$ and $C_{12}E_6$. The measurements were made in 0.1 M NaCl to reduce

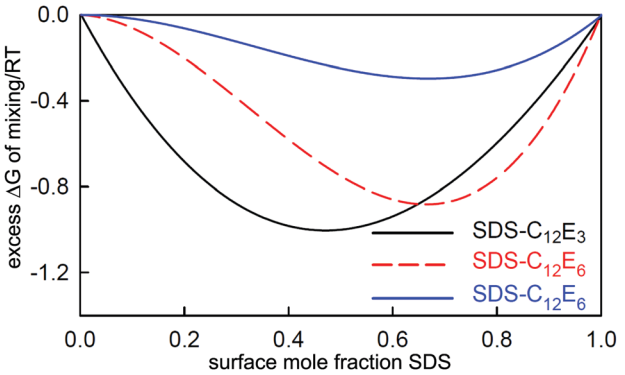

Fig. 14 Excess free energy of mixing *versus* surface composition (mole fraction of SDS) for SDS/$C_{12}E_3$, SDS/C_{12}E6 and SDS/$C_{12}E_8$ in 0.1 M NaCl. Redrawn from ref. 20.

the impacts of electrostatic repulsion and the large differences in CMC values, as well as to correspond more closely to the conditions in many formulations. Penfold and Thomas[20] more recently used the PPA to analyse the mixing properties of SDS/$C_{12}E_3$ and SDS/$C_{12}E_6$, along with some more recent measurements for SDS/$C_{12}E_8$.[112,123] Analysis of the CMC variation and the surface composition, both as a function of surfactant concentration and solution composition, required the inclusion of quadratic and cubic terms in the expansion of the excess free energy of mixing, ΔG_E. The variation of the free energy of mixing for the three systems is shown in Fig. 14, and the PPA parameters together with the minimum values of the excess free energy of mixing, ΔG_E(min), and the compositions at the minimum, x_{SDS}(min), for surface mixing are given in Table 1. All three mixtures have a relatively strong synergistic (attractive) interaction arising from the reduction of the electrostatic repulsion due to the inclusion of the nonionic component. This is further reduced by the presence of 0.1 M NaCl, and its specific impact is discussed later. The asymmetrical interaction with respect to the surface composition is clear in Fig. 14 and from the parameters in Table 1. The value of ΔG_E(min) at the surface shifts from close to symmetrical for SDS/$C_{12}E_3$to distinctly asymmetrical for SDS with either $C_{12}E_6$or $C_{12}E_8$, and its value is increasingly reduced as the EO chain length increases. In an ordered 2-D mixture of charged and uncharged species in the absence of electrolyte the simplest arrangement for minimising the electrostatic repulsions is a 1 : 2 ionic : nonionic ratio, as discussed elsewhere.[99,102] However the asymmetry in the mixing will depend upon electrostatic interactions, differences in packing requirements and changes in hydration. In electrolyte, the electrostatic interactions will be less dominant and the results here indicate a significant contribution from packing requirements and changes in hydration. The decreasing synergy, as shown by ΔG_E(min) implies an increasing packing constraint as the EO chain length increases. Furthermore the strength of the interaction is weaker for the micelles than the surface and this implies that the packing constraints are less severe in the micelle than at the surface. This was in part confirmed by Penfold *et al.*[124] in a study of the impact of the nonionic headgroup size on the mixed SDS/nonionic surfactant micelle structure.

As part of a wider study on ternary surfactant mixtures Liley *et al.*[123] also explored the impact of electrolyte on the surface and micelle mixing of the SDS/$C_{12}E_8$ mixture. The key PPA parameters from the analysis of the NR and CMC data are summarised in Table 2 together with values of the ΔG_E(min) for *surface* mixing, and the compositions at the minimum, x_{SDS}(min). This direct comparison shows a clear effect of electrolyte on the mixing properties. In the absence of salt the optimal mixing ratio is 2 : 1 nonionic : ionic, consistent with previous arguments, and consistent with the dominance of the electrostatic interaction. This is reinforced by the stronger interaction in the absence of electrolyte with ΔG_E(min) $\approx -0.9RT$. On the addition of electrolyte ΔG_E(min) is significantly reduced and the optimal composition is also quite different, reflecting the suppression of the electrostatic interaction and the now greater significance of the packing constraints. In contrast, the addition of electrolyte has little impact upon the micelle mixing parameters.

As a precursor to a study of the more complex ternary and quinary mixtures, the mixing of two different anionic surfactants, LAS and SLES, with $C_{12}E_8$ was studied by Liley *et al.*[112,123] This also provided the opportunity to probe the impact of changing the molecular structure of the anionic surfactant on the mixing. SLES is similar to SDS but has a short E_2 chain between the alkyl chain and sulfate headgroup. LAS has a dialkyl chain structure and a bulkier headgroup which includes a phenyl ring. Table 3 summarises the key PPA parameters obtained from the analysis of the NR and CMC data for $C_{12}E_8$ mixed with SDS, SLES, and LAS, in the absence and presence of 0.1 M NaCl. It is important to note that the sign of the cubic term changes according to which surfactant the coordinate x refers. In all three tables here x refers to the first named surfactant. Thus the sign is reversed between SDS-$C_{12}E_8$ and $C_{12}E_8$-SDS in Tables 2 and 3.

Broadly similar trends are observed for all three anionic surfactants when mixed with the nonionic $C_{12}E_8$. The synergy in the surface mixing is stronger than for the micelle mixing, as previously discussed. The impact of electrolyte is to reduce the synergistic effect and change the value of x_{SDS} (s)(min), consistent with the change from an interaction dominated by

Table 1 SDS-nonionic mixing parameters in 0.1M NaCl (units of RT)

mixture	B_m	C_m	B_s	C_s	x_{SDS} (s)(min)	ΔG_E (s)(min)
SDS/$C_{12}E_3$	−1.4	+1.4	−4.0	+0.5	0.47	−1.0
SDS/$C_{12}E_6$	−2.0	−2.0	−3.0	−2.9	0.67	−0.9
SDS/$C_{12}E_8$	−1.0	+1.0	−1.0	−1.0	0.67	−0.3

Table 2 SDS-$C_{12}E_8$ mixing properties with and without 0.1 M NaCl

Solution	B_m	C_m	B_s	C_s	x_{SDS} (s)(min)	ΔG_E (s)(min)
No salt	−1.0	+1.0	−3.0	+2.9	0.33	−0.9
0.1 M NaCl	−1.0	+1.0	−1.0	−1.0	0.67	−0.3

Table 3 $C_{12}E_8$ mixing properties with SDS, SLES and LAS with and without 0.1M NaCl. x refers to $C_{12}E_8$ throughout the Table

(a) No salt	B_m	C_m	x_m(min)	ΔG_E(min)
SDS	−1.0	−1.0	0.67	−0.3
SLES	−1.8	−1.8	0.67	−0.53
LAS	−2.6	−1.8	0.63	−0.72
Surface	**B_s**	**C_s**	**x_s(min)**	**ΔG_E(min)**
SDS	−3.0	−3.0	0.67	−0.89
SLES	−2.0	−2.0	0.67	−0.59
LAS	−4.4	−0.8	0.54	−1.1
(b) 0.1 M NaCl	B_m	C_m	x_m(min)	ΔG_E(min)
SDS	−1.0	−1.0	0.67	−0.3
SLES	0	0	—	—
LAS	−0.6	−0.6	0.67	−0.18
Surface	**B_s**	**C_s**	**x_s(min)**	**ΔG_E(min)**
SDS	−1.0	+1.0	0.33	−0.3
SLES	−0.3	+0.3	0.33	−0.09
LAS	−2.2	−1.0	0.6	−0.58

electrostatic repulsion to one dominated by steric or packing constraints. However the differences for the different anionic structures are significant. In the absence of salt the strength of the synergistic interaction at the surface is in the sequence LAS > SDS > SLES. This in part reflects the greater steric or packing contribution associated with the LAS dialkyl chain and the bulkier headgroup structures. SLES exhibits the lowest interaction strength, and this is in part associated with the weaker ionic nature of SLES compared with SDS or LAS, as reported by Xu *et al.*[43,44] The addition of electrolyte to all three mixtures also has a significant impact, and implies larger steric or packing constraints for LAS.

In the discussion above of nonionic surfactant mixing it was observed that although the saponin, escin, behaves predominantly like a nonionic surfactant, its different molecular structure gives rise to non-ideal mixing. This was explored further by Tucker *et al.*,[125] who investigated the mixing of escin with SDS, in the presence of electrolyte. The mixing was highly asymmetrical and synergistic, broadly consistent with the mixing of other nonionic/ionic mixtures. In this case the micelle mixing was more non-ideal than the surface and reflects the greater influence of the steric contribution due the rather different saponin structure compared to conventional surfactants.

The zwitterionic surfactants are an important class of surfactants, in that they have no overall charge but interact strongly with ionic surfactants. Their amphoteric nature results in a weaker interaction with biomaterials, and they are widely used in personal care formulations. Li *et al.*[126] used NR and ST to investigate the surface properties of a series of mixtures, SDS and C_{12}TAB, with two different zwitterionic surfactants dodecyldimethyl ammonium propane sulfonate, C_{12}SB, and dodecyldimethyl ammonium acetate, C_{12}CB. The interaction between SDS and C_{12}SB was particularly strong and ΔG_E highly asymmetric, as shown in Fig. 15. The asymmetry was characterised by the series expansion of ΔG_E up to and including the

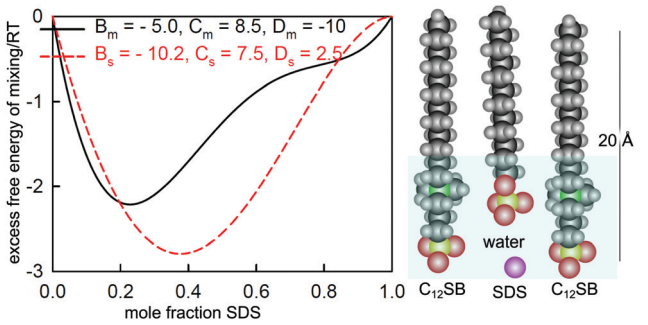

Fig. 15 Dependence of the excess free energy of mixing for surface and micelles on the composition of SDS-C_{12}SB mixtures, and a suggested molecular packing arrangement at the A–W interface. Redrawn from Li *et al.*[126]

quartic term. ΔG_E(min) for the surface occurred at a SDS mole fraction of 0.35 and a depth of −2.8 RT. The micellar interaction was weaker and more asymmetric, with ΔG_E(min) = $-2.2RT$ at an SDS composition of 0.23. Li *et al.*[126] observed that the strong synergistic interaction resulted in a strong peak in the total adsorption with composition, due to a significant increase in the packing in the mixed monolayer. The more efficient packing results from a structural rearrangement at the interface, which provides an effective reduction in the electrostatic repulsion, along the lines of the arrangement in Fig. 15. Significant differences in the packing constraints at the surface and in the micelles results in a marked difference in behaviour at the surface and in the micelles as also summarised in Fig. 15.

3.3 Ternary mixtures

Liley *et al.*[112] used NR to explore the surface mixing in the ternary surfactant mixture, SLES/LAS/$C_{12}E_8$; a surfactant mixture which represents the base formulation used in a wide range of home and personal care products. The micelle properties were evaluated on the basis of variations in the the mixed CMC, while the surface properties were investigated using NR measurements for concentrations above the CMC. A series of binary and ternary measurements were made as mapped out on the ternary diagram in Fig. 16.

The PPA interaction parameters were determined from the binary pairs. The asymmetry in the interactions required both

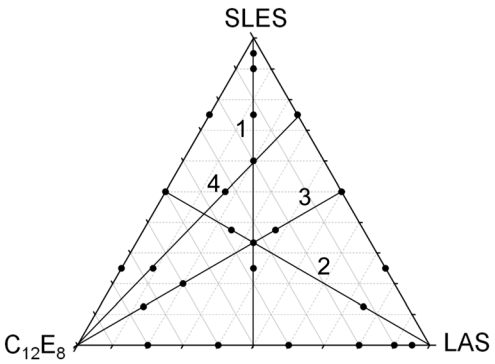

Fig. 16 Ternary diagram for SLES/LAS/$C_{12}E_8$ mixture, indicating the compositions at which NR measurements were made.

quadratic and cubic terms in the expansion of the excess free energy of mixing. The nature of the interactions for the anionic/nonionic pairs have been discussed earlier, and all three pairwise interactions are relatively weak. The interactions are dominated by the LAS/$C_{12}E_8$ interaction, for which $\Delta G_E(\min) \approx -1.1RT$, and the SLES/$C_{12}E_8$ and SLES/LAS interactions are weaker and comparable at $\Delta G_E(\min) \approx -0.6RT$. Although $\Delta G_E(\min)$ for the SLES/$C_{12}E_8$ and SLES/LAS interactions occurs close to a 2 : 1 nonionic:anionic ratio, it is close to equimolar for LAS/$C_{12}E_8$. This indicates a significant contribution from steric constraints associated with the packing at the interface. The stronger LAS/$C_{12}E_8$ interaction results in the surface adsorption being dominated by the $C_{12}E_8$ and LAS, and there is little SLES at the interface. This is illustrated graphically in Fig. 17, where the PPA interaction parameters are used to reproduce the ternary behaviour at the interface at a fixed surfactant concentration of 2 mM. Importantly the binary interaction parameters provide, without further adjustment, a moderately accurate distribution of the experimental adsorbed fractions for the ternary mixture.

Liley *et al.*[123] also explored the impact of electrolyte on the same ternary mixture. The addition of electrolyte, as discussed in the context of the binary mixtures earlier, weakens the synergistic interactions between SLES/$C_{12}E_8$ and LAS/$C_{12}E_8$. The SLES/LAS interaction, however, is hardly affected by the addition of electrolyte. These changes highlight the relative contributions of electrostatic and structural or packing factors. They also result in the surface of the ternary mixture being less strongly dominated by $C_{12}E_8$ and LAS adsorption, and consequently there is a greater adsorbed fraction of SLES at the interface. Importantly, these observations and comparisons show how manipulating the pairwise interactions through structural changes or the addition of electrolyte can impact directly upon the surface properties.

3.4 Quinary mixtures

The increasing interest in the use of biosurfactants in the development of more biosustainable and biodegradable surfactant based products has led to extensive studies of the R1–R2 rhamnolipid system from *Pseudomonas aeruginosa* bacteria and already examined in Fig. 12. Liley *et al.*[113] have used NR to investigate the adsorption properties of a quinary mixture, in which 30 mole%, of the ternary mixture SLES/LAS/$C_{12}E_8$ mixture is replaced by the rhamnolipid mixture R1/R2. The quinary mixture has been shown to be a highly effective surfactant mixture in detergency related applications. It is characterised by strong surface interactions but weaker micelle interactions, in which R1 dominates the surface adsorption. The quinary behaviour is well characterised by the respective pairwise PPA interactions which require quadratic and cubic terms in the expansion of the excess free energy of mixing. A unique set of surface and micelle interaction parameters describe the binary, ternary and quinary mixtures, as illustrated in Fig. 18 for the quinary mixture at two different R1:R2 ratios.

A significant proportion of the values of $\Delta G_E(\min)$ for the stronger interactions occur away from the regular solution value of $x(\min) = 0.5$, as shown in Table 4, due to the combination of electrostatic and steric contributions to the pairwise interactions. The best fits to the data are dominated by the strong interactions. This results in the dominance of R1 at the interface and a greater adsorption of SLES at the interface

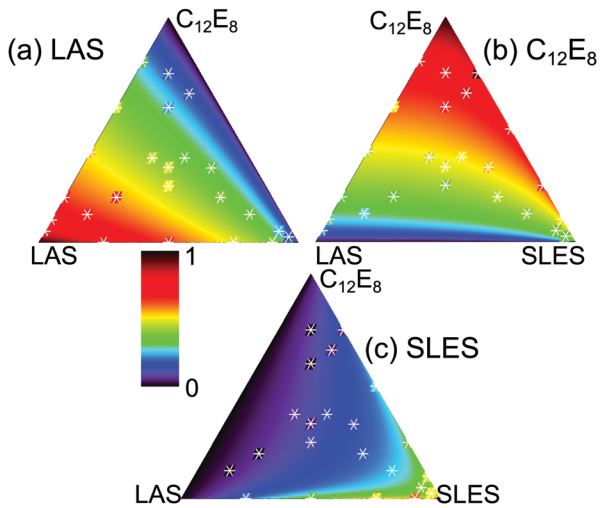

Fig. 17 Composition of the adsorbed layer for the ternary SLES/LAS/$C_{12}E_8$ mixture at a solution concentration of 2 mM. Each triangular diagram, (a)–(c) represents the distribution of the adsorbed fraction of each component using the PPA parameters derived from the binary interactions. The data points are white asterisks on a coloured spot, which disappears when there is exact agreement between experiment and calculation. Redrawn from Liley *et al.*[112]

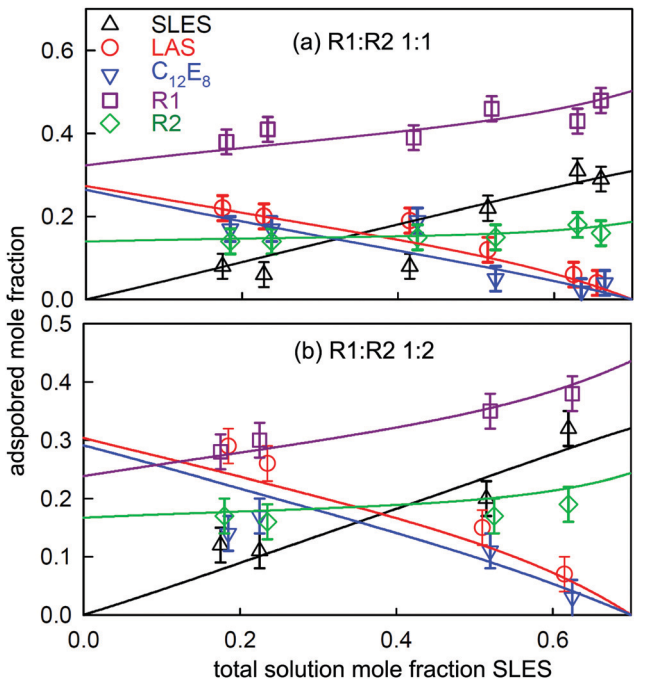

Fig. 18 Variation in adsorbed mole fraction for each component in the quinary mixture, SLES/LAS/$C_{12}E_8$/R1/R2, containing fixed mole fractions of R1 and R2. Reproduced by permission from Liley *et al.*[113]

Table 4 PPA parameters for the 10 binary interactions in the quinary SLES/LAS/$C_{12}E_8$/R1/R2 mixture. x_s refers to the first named surfactant in each case

Mixture	ΔG_E(min)	x_s(min)
LAS-R1	−0.3	0.46
$C_{12}E_8$-R1	−0.38	0.55
SLES-R1	−0.81	0.55
R1-R2	−0.48	0.65
LAS-R2	−0.24	0.67
$C_{12}E_8$-R2	0.0	(0.5)
SLES-R2	−0.24	0.33
SLES-LAS	−0.59	0.61
LAS-$C_{12}E_8$	−1.11	0.46
SLES-$C_{12}E_8$	−0.59	0.33

compared with that observed in the SLES/LAS/$C_{12}E_8$ mixture. This study is important in that it demonstrates the extent to which NR can be used to investigate the adsorption of complex multi-component mixtures. It illustrates the applicability of the PPA, the role of pairwise interactions and the ability to replicate complex variations in the surface composition. The detailed characterisation of the surface composition and quantification of the strength of the interactions provides important insights into the effectiveness of such mixtures which result primarily from the dominance of R1 at the interface.

3.5 Mixtures at the limit of the applicability of the PPA

Tucker *et al.*[35,128–130] extensively studied the self-assembly and adsorption properties of the dialkyl chain cationic surfactant, dihexadecyl dimethyl ammonium bromide, DHDAB, mixed with a range of different nonionic surfactants. Such mixtures are important as they are representative of the surfactant ingredients in the formulations associated with hair and clothes care products and conditioners. The mixtures exhibited a rich pattern of structures in their bulk phase behaviour, and this impacts directly upon their adsorption properties. In solution DHDAB has a low or zero preferred spontaneous curvature and forms planar lamellar or vesicular structures. The nonionic cosurfactants explored, $C_{12}E_3$, $C_{12}E_6$ and $C_{12}E_{12}$, have an increasing spontaneous curvature, and their structures vary from planar to globular structures. For $C_{12}E_6$ and $C_{12}E_{12}$ their mixing with DHDAB results in a transition from planar structures, lamellae and vesicles, to globular micelles, *via* an extensive mixed phase region which depends upon solution concentration, and composition, and co-surfactant type. For the DHDAB/$C_{12}E_3$ mixture the preference for planar structures for both components results in planar structures with varying membrane rigidity across the entire composition range. The structural changes result in an extreme behaviour in the surface adsorption, as shown in Fig. 19(a). The surface mixing is highly non-ideal and for all three mixtures there is a solution composition threshold below which there is no measurable adsorption of the nonionic component at the interface. This threshold increases in the nonionic solution composition as the EO group of the nonionic component increases from 3 to 6 to 12. For $C_{12}E_6$ and $C_{12}E_{12}$ beyond the threshold, the nonionic mole fraction at the surface increases sharply, and is quite different

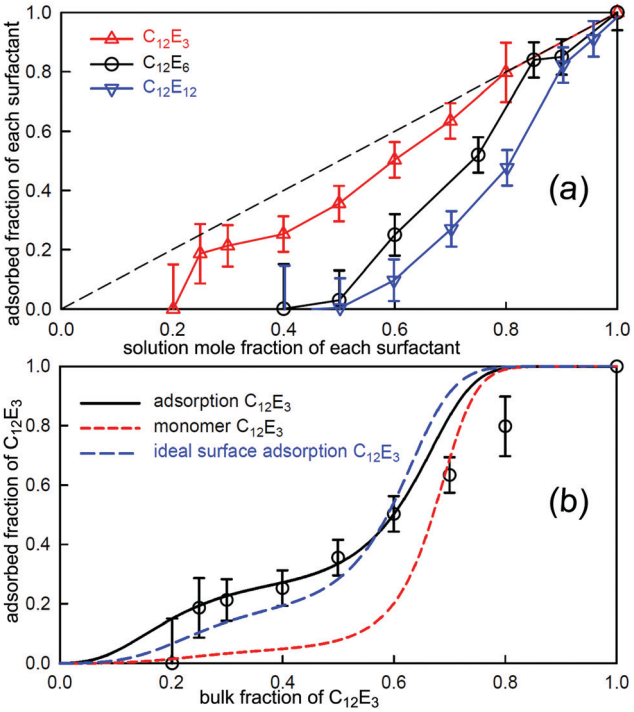

Fig. 19 (a) Surface composition (mole fraction of nonionic) *versus* solution composition for 1.5 mM DHDAB/$C_{12}E_3$, $C_{12}E_6$ and $C_{12}E_{12}$. The lines are a guide to the eye only. (b) Variation in surface composition (mole fraction $C_{12}E_3$) with bulk solution composition for 1.5 mM DHDAB/$C_{12}E_3$. The lines are PPA calculations using the interaction parameters B_m = −6.5, C_m = −5.0, D_m = −5.0, B_s = −1.2, C_s = 0.3, and D_s = −0.3. The three surface parameters were set to zero for the ideal adsorption calculation. Redrawn from ref. 127.

to the general patterns of behaviour observed in many other mixtures. The pattern of behaviour for the DHDAB/$C_{12}E_3$ mixture is closer to that encountered in other surfactant mixtures. The general form of these adsorption patterns imply that below the composition threshold the nonionic monomer concentration is low and that the nonionic surfactant is mostly incorporated into the bulk aggregates.

The sharp transition implies that the mixing parameters and interactions are highly asymmetrical. Penfold and Thomas[127] explored the extent to which the PPA with the higher order terms, quadratic, cubic and quartic, in the series expansion of the excess free energy of mixing can replicate these features. The PPA broadly reproduces the main features of the adsorption of DHDAB/$C_{12}E_3$, as shown in Fig. 19(b) for the micelle and surface interaction parameters given in the figure caption. The extreme asymmetry required interaction parameters expanded to include the quartic term. The parameters imply that the surface mixing is close to ideal and that the surface composition is driven almost entirely by the bulk aggregation. Such large negative interaction parameters also imply that the system is close to phase separation. This could be within the same aggregated phase or as two separate phases; however, this is not evident from the observed bulk phase behaviour. It was not possible to obtain a meaningful description of the adsorption data for DHDAB mixed with $C_{12}E_6$ or $C_{12}E_{12}$. This suggests

that the PPA and the expansion of the excess free energy of mixing in terms of a series is inadequate when the aggregated phases are more structured lamellar, hexagonal or cubic phases and where distinct changes between these different structures exist.

The solubilisation and co-adsorption at interfaces of small molecules, hydrotopes, such as perfumes, flavours, dyes, and drug molecules, are key aspects of the application of surfactants in detergency, cosmetics, foods, pesticides, and drug delivery. Bradbury *et al.*[131] used NR to investigate the adsorption of perfume molecules by co-adsorption with the anionic surfactant LAS at the air–water interface. Their focus was on two model perfumes, phenyl ethanol, PE, and linalool, LL, with differing degrees of hydrophobicity and hydrophilicity, where PE is characteristic of a more hydrophilic perfume molecule and LL of a more hydrophobic one. This is reflected in their different log$P$ values, 1.45 and 3.3. They also have quite different limiting solubilities, 150 and 10 mM respectively. What is particularly interesting and relevant to this review is the extent to which the non-ideal treatment of surfactant mixing applies. The variation in the LAS CMC with the addition of PE or LL was analysed assuming that the PPA model is valid when the effective CMC values are taken to be the limiting solubilities. Interaction parameters of B = +1.0 for LL and −4.0 for PE provide an adequate description of the CMC variation but the extensions to the calculation of the surface composition are less successful. The fuller PPA calculations imply that LAS/LL mixing is unfavourable and relatively close to ideal mixing, whereas LAS/PE mixing is less ideal and there is some synergy. The variation in the surface composition with solution composition for LAS/LL and LAS/PE (Fig. 20(b)) is well explained by the combination of the PPA and the use of the limiting solubility as the effective CMC. It also shows that the more hydrophobic LL competes more effectively for the surface than the relatively hydrophilic PE. Fig. 20(c) further shows that the optimum composition of the surface corresponds to a relatively low fraction of perfume, about 1/4 to 1/3, in the surface layer. This is consistent with the perfume requiring the hydrophobic environment of a relatively well packed surfactant layer in order to remain at the surface.

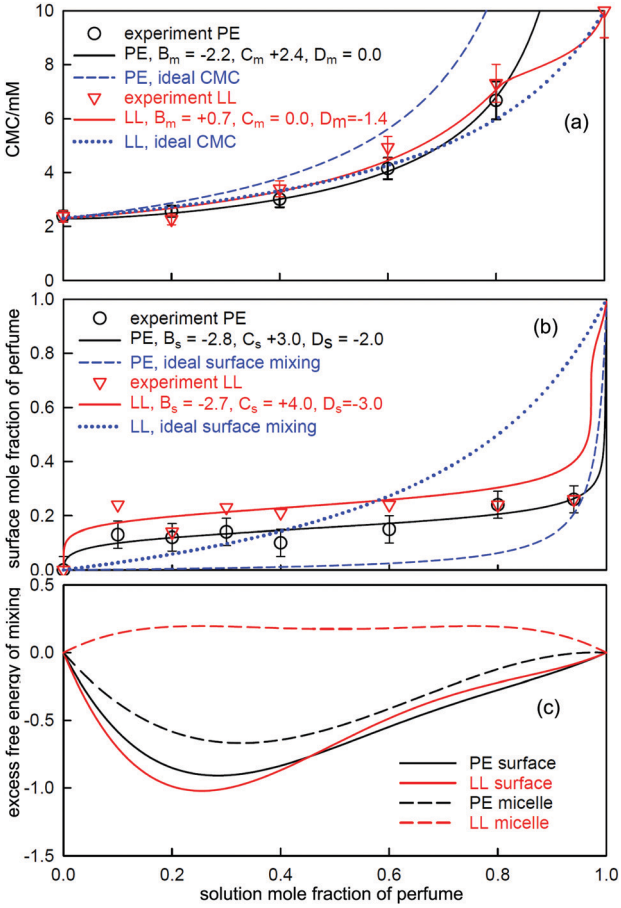

Fig. 20 Variation in (a) CMC and (b) surface composition for LL/6LAS and PE/6LAS with solution mole fraction of perfume. The calculated lines are continuous for PPA calculations with the parameters given in the diagram and dashed for ideal micellar mixing. (c) Excess free energy of mixing for micellar solutions and at the surface. The data are from ref. 131.

3.6 Summary and wider implications

For a long time the Gibbs equation has been used primarily to analyse ST behaviour to determine surface excesses at A–W and water–oil interfaces. However, its correct application requires a knowledge of the composition of the surface layer, which, because of the extremely low levels of impurity required to cover the surface, is often uncertain. NR is the first method to be able to determine directly the adsorbed amount of a given species at the A–W interface, either on its own or in a mixture. Not surprisingly the combination of NR and ST measurements both solves some previous observed anomalies and identifies some new ones. The anomalies are of several types. Contamination of the surface by nonionic impurities can be studied directly. Contamination by ionic impurities, which is a widely occurring phenomenon and which NR does not observe directly, can nevertheless be identified clearly by combining NR and ST. Comparison of NR and ST also clearly identifies the onset of depletion, which has previously been mistaken for the onset of aggregation in the bulk solution. Finally, unlike the Gibbs equation, NR measurements are not affected by situations where the activity and concentration are not the same, *e.g.* above the CMC. This leads to a further set of situations where comparison of NR and Gibbs gives important information about the state of the adsorbed species in the bulk solution.

The most important feature of NR is its ability to determine the surface composition of mixtures above and below the CMC. Most formulations used in practice are carefully chosen mixtures and their optimum operation is often at concentrations above the CMC. The extensive range of data on surface and micelle mixing that can now be obtained from NR and the related small angle neutron scattering (SANS) has enabled a more detailed evaluation of the thermodynamics of surfactant mixing using the pseudophase approximation (PPA). The data is of a quality that makes it possible to include higher order terms in the series expansion of the excess free energy of mixing. As a result, it is now possible to use a global set of

interaction parameters to describe all the data associated with a particular mixture and this provides a more accurate and relevant description of both surface and micellar mixing. This has been extensively demonstrated in a range of binary mixtures, which include nonionic mixtures and ionic nonionic mixtures, and has been extended to ternary and quinary mixtures. The analysis of the multicomponent mixtures here shows that pairwise interactions in both surface and micellar mixing are sufficient to describe mixtures with greater than two components. This is an important advance and allows the behaviour of more complex multicomponent mixtures to be predicted solely on the basis of the interactions between their different binary components. Limits to the range of application only start to appear when there is phase separation in either micelle or surface, as shown for DHDAB/nonionic and surfactant/perfume mixtures. The developments in the evaluation of surfactant mixing described in this review should provide both a framework in which a wider variety of multicomponent mixtures can be investigated and a basis for reaching a deeper theoretical understanding.

Author contributions

The authors contributed equally to all parts of this manuscript.

Conflicts of interest

There are no conflicts to declare.

Notes and references

1 J. R. Lu, E. M. Lee, R. K. Thomas, J. Penfold and S. L. Flitsch, *Langmuir*, 1993, **9**, 1352–1360.
2 T. Crowley, E. Lee, E. Simister and R. Thomas, *Phys. B*, 1991, **173**, 143–156.
3 J. R. Lu, R. K. Thomas and J. Penfold, *Adv. Colloid Interface Sci.*, 2000, **84**, 143–304.
4 J. R. Lu, R. K. Thomas, B. P. Binks, D. Crichton, P. D. I. Fletcher, J. R. McNab and J. Penfold, *J. Phys. Chem. B*, 1998, **102**, 5785–5793.
5 J. R. Lu, T. J. Su, Z. X. Li, R. K. Thomas, E. J. Staples, I. Tucker and J. Penfold, *J. Phys. Chem.*, 1997, **101**, 10332–10339.
6 A. Shahir, K. Nguyen and A. Nguyen, *Phys. Chem. Chem. Phys.*, 2016, **18**, 8794–8805.
7 A. Shahir, D. Arabadzhieva, H. Petkova, S. Karakashev, A. Nguyen and E. Mileva, *J. Phys. Chem. C*, 2017, **121**, 11472–11487.
8 M. Peng, T. Duignan, C. Nguyen and A. Nguyen, *Langmuir*, 2021, **37**, 2237–2255.
9 Z. Li, R. Thomas, A. Rennie and J. Penfold, *J. Chem. Soc., Faraday Trans.*, 1996, **92**, 565–572.
10 Z. Li, R. Thomas, A. Rennie and J. Penfold, *J. Phys. Chem. B*, 1998, **102**, 185–192.
11 T. Su, R. Thomas and J. Penfold, *Langmuir*, 1997, **13**, 2133–2142.
12 Z. Li, C. Bain, R. Thomas, D. Duffy and J. Penfold, *J. Phys. Chem. B*, 1998, **102**, 9473–9480.
13 C. J. Radke, *Adv. Colloid Interface Sci.*, 2015, **222**, 600–614.
14 S. Ikeda, *Adv. Colloid Interface Sci.*, 1982, **18**, 93–130.
15 F. M. Menger, L. Shi and S. A. A. Rizvi, *J. Am. Chem. Soc.*, 2009, **131**, 10380–10831.
16 P. Li, Z. Li, H. Shen, R. Thomas, J. Penfold and J. Lu, *Langmuir*, 2013, **29**, 9324–9334.
17 H. Xu, P. X. Li, K. Ma, R. K. Thomas, J. Penfold and J. R. Lu, *Langmuir*, 2013, **29**, 9324–9334.
18 P. X. Li, R. K. Thomas and J. Penfold, *Langmuir*, 2014, **30**, 6739–6747.
19 E. Hutchinson, *J. Colloid Sci.*, 1948, **3**, 413–414.
20 J. Penfold and R. Thomas, *Mol. Phys.*, 2019, **117**, 3376–3388.
21 R. Defay, I. Prigogine, A. Bellemans and D. H. Everett, *Surface Tension and Adsorption*, Longman, London, 1966.
22 J. R. Lu, I. P. Purcell, E. M. Lee, E. A. Simister, R. K. Thomas, A. R. Rennie and J. Penfold, *J. Colloid Interface Sci.*, 1995, **174**, 441–455.
23 H. Liu, X. Hua, Z. Li, K. Fa, H. Gong, K. Ma, M. Liao, P. Li, J. Webster, J. Petkov, R. Thomas and J. Lu, *J. Colloid Interface Sci.*, 2021, **591**, 106114.
24 P. A. Kralchevsky, K. D. Danov, V. L. Kolev, G. Broze and A. Mehreteab, *Langmuir*, 2003, **19**, 5004–5018.
25 Z. Li, J. Lu and R. Thomas, *Langmuir*, 1997, **13**, 3681–3685.
26 Z. Li, E. Lee, R. Thomas and J. Penfold, *J. Colloid Interface Sci.*, 1997, **187**, 492–497.
27 K. Shinoda and H. Nakayama, *J. Colloid Interface Sci.*, 1963, **18**, 705–712.
28 D. G. Hall, B. A. Pethica and K. Shinoda, *Bull. Chem. Soc. Jpn.*, 1975, **48**, 324–326.
29 S. W. An, J. R. Lu, R. K. Thomas and J. Penfold, *Langmuir*, 1996, **12**, 2446–2453.
30 K. Lunkenheimer, K. Geggel and D. Prescher, *Langmuir*, 2017, **33**, 10216–10224.
31 P. Linse and T. A. Hatton, *Langmuir*, 1997, **13**, 4066–4078.
32 J. B. Vieira, Z. X. Li and R. K. Thomas, *J. Phys. Chem. B*, 2002, **106**, 5400–5407.
33 C. Phan, S. Yusa, T. Honda, K. Sharker, A. Hyde and C. Nguyen, *ACS Omega*, 2018, **3**, 10907–10911.
34 S. An, R. Thomas, C. Forder, N. C. Billingham, S. P. Armes and J. Penfold, *Langmuir*, 2002, **18**, 5064–5073.
35 I. Tucker, J. Penfold, R. Thomas, I. Grillo, J. Barker and D. Mildner, *Langmuir*, 2008, **24**, 6509–6520.
36 J. Penfold, R. Thomas, P. Li, J. Petkov, I. Tucker, J. Webster and A. Terry, *Langmuir*, 2015, **31**, 3003–3011.
37 J. A. de Feijter and J. Benjamins, *J. Colloid Interface Sci.*, 1981, **81**, 91–107.
38 P. H. Elworthy and K. J. Mysels, *J. Colloid Interface Sci.*, 1966, **21**, 331–347.
39 T. Sasaki, M. Hattori, J. Sasaki and K. Nukina, *Bull. Chem. Soc. Jpn.*, 1975, **48**, 1397–1403.
40 S. G. Cutler, P. Meares and D. G. Hall, *J. Chem. Soc., Faraday Trans. I*, 1978, **74**, 1758–1767.

41 J. Lu, E. Simister, R. Thomas and J. Penfold, *J. Phys. Chem.*, 1993, **97**, 13907–13913.
42 R. Alargova, J. Petkov, D. Petsev, I. B. Ivanov, G. Broze and A. Mehreteab, *Langmuir*, 1995, **11**, 1530–1536.
43 H. Xu, J. Penfold, R. K. Thomas, J. T. Petkov, I. Tucker and J. P. R. Webster, *Langmuir*, 2013, **29**, 11656–11666.
44 H. Xu, J. Penfold, R. K. Thomas, J. T. Petkov, I. Tucker and J. P. R. Webster, *Langmuir*, 2013, **29**, 12744–12753.
45 H. Xu, J. Penfold, R. K. Thomas, J. T. Petkov, I. Tucker, I. Grillo and A. Terry, *Langmuir*, 2013, **29**, 13359–13366.
46 P. Li, J. Penfold, R. Thomas and H. Xu, *Adv. Colloid Interface Sci.*, 2019, **269**, 43–86.
47 Z. Wang, P. Li, K. Ma, Y. Chen, J. Webster, M. Campana, Z. Yan, J. Penfold and R. Thomas, *J. Colloid Interface Sci.*, 2021, **597**, 223–232.
48 P. Li, Z. Wang, K. Ma, Y. Chen, Z. Yan, J. Penfold, R. Thomas, M. Campana, J. Webster and A. Washington, *J. Colloid Interface Sci.*, 2020, **565**, 567–581.
49 I. Tucker, J. Penfold, R. Thomas, C. Dong, S. Golding, C. Gibson and I. Grillo, *Langmuir*, 2010, **26**, 10614–10626.
50 I. Tucker, J. Penfold, R. Thomas, C. Dong, S. Golding, C. Gibson and I. Grillo, *Langmuir*, 2011, **27**, 6674–6682.
51 H. Xu, J. Penfold, R. K. Thomas, J. T. Petkov, I. Tucker, J. P. R. Webster, I. Grillo and A. Terry, *Langmuir*, 2014, **30**, 4694–4702.
52 R. Alargova, K. Danov, J. Petkov, P. Kralchevsky, G. Broze and A. Mehreteab, *Langmuir*, 1997, **13**, 5544–5551.
53 J. Penfold, R. Thomas, X. Zhang and D. Taylor, *Langmuir*, 2009, **25**, 3972–3980.
54 S. Halacheva, J. Penfold, R. Thomas and J. Webster, *Langmuir*, 2013, **29**, 5832–5840.
55 J. Penfold, R. Thomas and P. Li, *J. Colloid Interface Sci.*, 2016, **463**, 199–206.
56 F. M. Menger and L. Shi, *J. Am. Chem. Soc.*, 2009, **131**, 6672–6673.
57 L. X. Jiang, J. B. Huang, A. Bahramian, P. X. Li, R. K. Thomas and J. Penfold, *Langmuir*, 2012, **28**, 327–338.
58 R. Meszaros, L. Thompson, M. Bos, I. Varga and T. Gilanyi, *Langmuir*, 2003, **19**, 609–615.
59 C. Phan, C. Nguyen, H. Nakahara, O. Shibata and T. Nguyen, *Langmuir*, 2016, **32**, 12842–12847.
60 A. Bahramian, R. K. Thomas and J. Penfold, *J. Phys. Chem. B*, 2014, **118**, 2769–2783.
61 J. Penfold and R. Thomas, *J. Phys. Chem. B*, 2020, **124**, 6074–6094.
62 D. J. F. Taylor, R. K. Thomas and J. Penfold, *Langmuir*, 2002, **18**, 4748–4757.
63 J. Penfold, I. Tucker, R. Thomas, D. Taylor, X. Zhang, C. Bell, C. Breward and P. Howell, *Langmuir*, 2007, **23**, 3128–3136.
64 P. Hansson and M. Almgren, *Langmuir*, 1994, **10**, 2115–2124.
65 K. Hayakawa and J. Kwak, *J. Phys. Chem.*, 1982, **86**, 3866–3870.
66 I. Prigogine, R. Defay, A. Bellemans and D. H. Everett, *Surface tension and adsorption, Chapter XXI, Sections 8 and 9*, Longman, London, 1966.
67 G. Manning, *Quart. Rev. Biophysics*, 1978, **11**, 179–246.
68 N. Ise and T. Okubo, *Macromolecules*, 1978, **11**, 439–447.
69 D. J. F. Taylor, R. K. Thomas, P. X. Li and J. Penfold, *Langmuir*, 2003, **19**, 3712–3719.
70 E. Staples, I. Tucker, J. Penfold, N. Warren, R. K. Thomas and D. J. F. Taylor, *Langmuir*, 2002, **18**, 5147–5153.
71 J. H. Buckingham, J. Lucassen and F. Hollway, *J. Colloid Interface Sci.*, 1978, **67**, 423–431.
72 A. J. Konop and R. H. Colby, *Langmuir*, 1999, **15**, 58–65.
73 D. J. F. Taylor, R. K. Thomas, P. X. Li and J. Penfold, *Langmuir*, 2003, **19**, 3712–3719.
74 I. Varga and R. A. Campbell, *Langmuir*, 2017, **33**, 5915–5924.
75 S. H. Myrick and E. I. Franses, *Colloids Surf., A*, 1998, **143**, 503–515.
76 S. Sitar, B. Goderis, P. Hansson and K. Kogej, *J. Phys. Chem. B*, 2012, **116**, 4634–4645.
77 R. G. Nause, D. A. Hoagland and H. H. Strey, *Macromolecules*, 2008, **41**, 4012–4019.
78 W. Al-Soufi, L. Pineiro and M. Novo, *J. Colloid Interface Sci.*, 2012, **370**, 102–110.
79 L. Song and M. Rosen, *Langmuir*, 1996, **12**, 1149–1153.
80 P. X. Li, C. C. Dong, R. K. Thomas, J. Penfold and Y. L. Wang, *Langmuir*, 2011, **27**, 2575–2586.
81 Z. X. Li, C. C. Dong and R. K. Thomas, *Langmuir*, 1999, **15**, 4392–4396.
82 E. Alami, G. Beinert, P. Marie and R. Zana, *Langmuir*, 1993, **9**, 1465–1467.
83 R. Zana, M. Benrraou and R. Rueff, *Langmuir*, 1991, **7**, 1072–1075.
84 R. Zana, *J. Colloid Interface Sci.*, 2002, **246**, 182–190.
85 R. Zana, *J. Colloid Interface Sci.*, 2002, **248**, 203–220.
86 J. Wegrzyska, G. Para, J. Chlebicki, P. Warszyski and K. Wilk, *Langmuir*, 2008, **24**, 3171–3180.
87 Y. Geng and L. S. Romsted, *J. Phys. Chem. B*, 2005, **109**, 23629–23637.
88 F. Menger and C. Littau, *J. Am. Chem. Soc.*, 1993, **115**, 10083–10090.
89 M. J. Rosen, J. H. Mathias and L. Davenport, *Langmuir*, 1999, **15**, 7340–7346.
90 B. Cai, J. Dong, L. Cheng, Z. Jiang, Y. Yang and X. Li, *Soft Matter*, 2013, **9**, 7637–7646.
91 F. François, D. Sarazin, T. Schwartz and G. Weill, *Polymer*, 1979, **20**(969), 975.
92 J. Zhang, R. Thomas and J. Penfold, *Langmuir*, 2020, **36**, 11661–11675.
93 J. H. Clint, *J. Chem. Soc., Faraday Trans. I*, 1975, **71**, 1327–1334.
94 D. N. Rubingh, *Solution Chemistry of Surfactants*, ed. K. L. Mittal, Plenum Press, New York, 1979, pp. 337–354.
95 P. Holland and D. Rubingh, *J. Phys. Chem.*, 1983, **87**, 1984–1990.
96 P. M. Holland, *Adv. Colloid Interface Sci.*, 1986, **26**, 111–129.
97 B. Ingram, *Colloid Polym. Sci.*, 1980, **258**, 191–192.
98 M. J. Rosen and X. Y. Hua, *J. Colloid Surf. Sci.*, 1982, **86**, 164–172.

99 I. Reif and P. Somasundaran, *Langmuir*, 1999, **15**, 3411–3417.
100 H. Maeda, *J. Phys. Chem. B*, 2005, **109**, 15933–15940.
101 J. D. Hines, R. K. Thomas, P. R. Garrett, G. K. Rennie and J. Penfold, *J. Phys. Chem. B*, 1998, **102**, 8834–8846.
102 A. Patist, S. Devi and D. O. Shah, *Langmuir*, 1999, **15**, 7403–7405.
103 J. A. V. Butler, *Proc. Royal Soc.*, 1932, **A135**, 348–375.
104 E. H. Lucassen-Reynders, *Progress Surface Membrane Science*, 1976, **10**, 253–360.
105 G. Kaptay, *Langmuir*, 2019, **35**, 10987–10992.
106 O. Redlich and A. T. Kister, *Ind. Eng. Chem.*, 1948, **40**, 345–348.
107 A. J. Jackson, P. X. Li, C. C. Dong, R. K. Thomas and J. Penfold, *Langmuir*, 2009, **25**, 3957–3965.
108 J. D. Hoffman, *Numerical Methods for Engineers and Scientists*, Marcel Dekker Inc, New York, 2nd edn, 2001.
109 P. Holland and D. N. Rubingh, *ACS Symp. Ser.*, 1992, **501**, 2–30.
110 J. A. Barker, *Australian J. Chem.*, 1953, **6**, 207–210.
111 J. S. Rowlinson and F. L. Swinton, *Liquids and Liquid Mixtures*, Butterworth-Heinemann Ltd, London, 3rd edn, 1982.
112 J. Liley, R. Thomas, J. Penfold, I. Tucker, J. Petkov, P. Stevenson and J. Webster, *J. Phys. Chem. B*, 2017, **121**, 2825–2838.
113 J. Liley, R. Thomas, J. Penfold, I. Tucker, J. Petkov, P. Stevenson, I. Banat, R. Marchant, M. Rudden and J. Webster, *Langmuir*, 2017, **33**, 13027–13039.
114 H. Xu, P. Li, K. Ma, R. Welbourn, J. Doutch, J. Penfold, R. Thomas, D. Roberts, J. Petkov, K. Choo and S. Khoo, *J. Colloid Interface Sci.*, 2018, **516**, 456–465.
115 Y. Nikas, S. Pruuvada and D. Blankschtein, *Langmuir*, 1992, **8**, 2680–2689.
116 Z. Wang, P. Li, K. Ma, Y. Chen, Z. Yan, J. Penfold, R. Thomas, M. Campana, J. Webster, Z. Li, H. Neil, J. H. Xu, J. Petkov and D. Roberts, *J. Colloid Interface Sci.*, 2021, 876–890.
117 J. Penfold, E. Staples, T. Crowley and I. Tucker, *Colloids Surf., A*, 1995, **102**, 127–132.
118 J. Penfold, E. Staples, I. Tucker, L. Thompson and R. Thomas, *J. Colloid Interface Sci.*, 2002, **247**, 404–411.
119 M. Chen, J. Penfold, R. Thomas, T. Smyth, A. Perfumo, R. Marchant, I. Banat, P. Stevenson, A. Parry, I. Tucker and I. Grillo, *Langmuir*, 2010, **26**, 18281–18292.
120 I. Tucker, A. Burley, R. Petkova, S. Hosking, R. Thomas, J. Penfold, P. Li, K. Ma, J. Webster and R. Welbourn, *J. Colloid Interface Sci.*, 2020, **574**, 385–393.
121 J. Penfold, E. Staples, L. Thompson, I. Tucker, J. Hines, R. Thomas and J. Lu, *Langmuir*, 1995, **11**, 2496–2503.
122 E. Staples, L. Thompson, I. Tucker, J. Penfold, R. Thomas and J. Lu, *Langmuir*, 1993, **9**, 1651–1656.
123 J. Liley, R. Thomas, J. Penfold, I. Tucker, J. Petkov, P. Stevenson and J. Webster, *Langmuir*, 2017, **33**, 4301–4312.
124 J. Penfold, I. Tucker, R. Thomas, E. Staples and R. Schuermann, *J. Phys. Chem. B*, 2005, **107**, 10760–10770.
125 I. Tucker, A. Burley, R. Petkova, S. Hosking, J. Penfold, R. Thomas, P. Li, J. Webster and R. Welbourn, *Langmuir*, 2020, **36**, 5997–6006.
126 P. Li, K. Ma, R. Thomas and J. Penfold, *J. Phys. Chem. B*, 2016, **120**, 3677–3691.
127 J. Penfold and R. Thomas, *Mol. Phys.*, 2019, **117**, 3376–3388.
128 I. Tucker, J. Penfold, R. Thomas, J. Barker and D. Mildner, *Langmuir*, 2008, **24**, 7674–7687.
129 I. Tucker, J. Penfold, R. Thomas, J. Barker and D. Mildner, *Langmuir*, 2008, **24**, 10089–10098.
130 J. Penfold, E. Staples, S. Ugazio, I. Tucker, L. Soubiran, J. Hubbard, M. Noro, B. O'Malley, A. Ferrante, G. Ford and H. Buron, *J. Phys. Chem. B*, 2005, **109**, 18107–18116.
131 R. Bradbury, J. Penfold, R. Thomas, I. Tucker, J. Petkov and C. Jones, *Langmuir*, 2013, **29**, 3361–3369.